2019

Stable Isotopes of Clay Minerals from Autoclave Tests of Oil Sands: Implications for Clay Formation during Steaming of Alberta Clearwater Oil Sands

Shaoneng He
Nanyang Technological University, Singapore

Fred J. Longstaffe
Western University, flongsta@uwo.ca

Zhihong Zhou
Alberta Innovates

1   Stable isotopes of clay minerals from autoclave tests of oil sands:

2   Implications for clay formation during steaming of Alberta Clearwater

3   oil sands

4

5   Shaoneng He[1*], Fred J. Longstaffe[2], Zhihong Zhou[3]

6   1. *Earth Observatory of Singapore, Nanyang Technological University, Singapore 639798*

7   2. *Department of Earth Sciences, The University of Western Ontario, London, Ontario,*

8   *Canada N6A 5B7*

9   3. *Clean Energy, Alberta Innovates, Edmonton, Alberta, Canada T6N 1E4*

10

11

12

13

14

15   * Corresponding author: Shaoneng He

16   Earth Observatory of Singapore, Nanyang Technological University, Singapore

17   639798

18   Email: snhe@ntu.edu.sg or heshaoneng@gmail.com

19

20

21

22   **ABSTRACT**: In an effort to evaluate mineral-water isotopic exchange during cyclic steam

23   stimulation (CSS), solutions and <2 μm berthierine-dominated solids from the Clearwater

24   Formation oil sands of Alberta, Canada were analyzed for stable isotope compositions before and

25   after reaction in autoclaves for 1008 hours at 250°C. There was no significant change in solution

26    $\delta^{18}O$ and δ^2H, which is consisten with the high water/mineral ratio used in the experiments. The

27   solids showed a marked decrease in both $\delta^{18}O$ and δ^2H following the experiments. Pre-run solids

28   have $\delta^{18}O$ of +9.5 to +12.9 ‰ and δ^2H of −114 to −113 ‰, whereas post-run solids have $\delta^{18}O$ of

29   −4.7 to +2.1 ‰ and δ^2H of −147 to −128 ‰. Neither oxygen- nor hydrogen-isotope equilibrium

30   was established between the solids and the solutions. Calculation suggests that oxygen-isotope

31   exchange (44-58%) was greater between the solids and solutions than was the case for hydrogen

32   isotopes (23 to 50 %). We propose that this behaviour resulted from partial inheritance of the

33   pre-run berthierine structure during formation of the post-run smectite, chlorite-smectite and

34   chlorite. This process confounds the use of clay mineral stable isotope compositions as a

35   temperature indicator of *in situ* steam/steam condensate interaction with oil-sands reservoirs.

36   The results also suggest an additional mechanism by which new clay minerals can be formed

37   during CSS-related, artificial diagenesis.

38

41

42

1. Introduction

The Province of Alberta, Canada, has the third largest proven oil reserves in the world, after Venezuela and Saudi Arabia, containing about 170 billions barrels of recoverable bitumen in-place in its oil sands (Giesy et al., 2010; Banerjee, 2012; Hashemi et al., 2014; Osacký et al., 2017; Alberta Energy, 2018). There are three major Alberta oil sands deposits, situated in the north-eastern portion of the province and covering an area of nearly 141,000 km^2: Athabasca, Peace River and Cold Lake (Fig. 1). The majority of the bitumen is hosted in unconsolidated Lower Cretaceous sands of the Mannville Group in the Western Canada Sedimentary Basin. In the Cold Lake area, the Clearwater Formation is the most prolific bitumen reservoir among the three units of the Cretaceous Mannville Group, which include the McMurray Formation, the Clearwater Formation and the Grand Rapids Formation (Wightman et al., 1989; Longstaffe, 1994; National Energy Board, 2000).

Hydrocarbons in the Alberta oil sands consist of highly viscous (exceeding 10,000 mPa•s), low API (8˚-12˚) heavy oil and bitumen (Chopra et al., 2010; Banerjee, 2012; Speight, 2016). The heavy oil and bitumen pose technical challenges during production because they are largely immobile under normal reservoir conditions. Since the Clearwater Formation is buried to depths of ~300 to 600 m (Hornibrook and Longstaffe, 1996; Sheng, 2013), open pit mining is not practical. Recovery of heavy oil and bitumen from the Clearwater oil sands therefore commonly involves *in situ* processes, such as cyclic steam stimulation (CSS), during which steam is injected into the oil sands reservior at temperatures ranging from 200 to 300°C (Beattie et al., 1991; Jiang et al., 2010; Banerjee, 2012; Sheng, 2013; Alvarez and Han, 2013). The high temperatures during CSS trigger reactions between the reservoir solids and injected fluids and formation waters. These reactions

65   have potential to cause formation damage – a decrease in permeability through formation of clay

66   minerals, precipitation of scale, and the physical migration of clay-size fines.

67
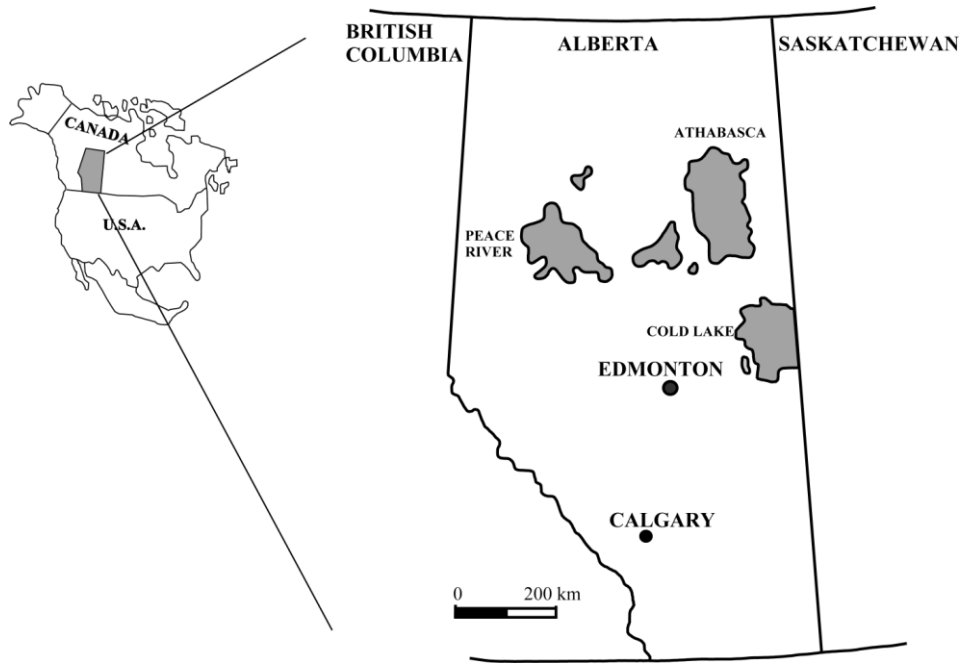
68

69   **Fig. 1.** Simplified map of Alberta with the locations of its three major oil sands deposits: Peace

70   River, Cold Lake and Athabasca. The samples examined in this study are from the Cold Lake

71   deposits.

72

73   The Clearwater deposits are very rich in clay minerals, which can comprise as much as 10

74   % of the sands (Zhou et al., 1994). Most of the Clearwater Formation facies contain abundant

75   detrital clays, which occur in interbeds, laminae and clasts as well as being dispersed in the matrix

76   (McCrimmon, 1996). The unit is also very rich in secondary clays (Longstaffe, 1994; Hornibrook

77   and Longstaffe, 1996; McKay and Longstaffe, 1997). The fine grain size, large surface area and

78   commonly grain-coating and/or pore-lining nature of these clays makes them more likely to react

79   with steam during CSS. As noted above, modification of clay minerals can cause significant

80   formation damage to reservoirs during hydrocarbon recovery (e.g., Gray and Rex, 1966; Kirk et al.,

81   1987; Krueger, 1988; Barrett and Mathias, 1992; Nadeau, 1998; Civan, 2016; Wilson et al., 2014).

82   These studies show that formation of swelling clay minerals in particular can cause a reduction in

83   porosity and permeability of reservoirs during thermal recovery. Remediation of such formation

84   damage is usually costly and difficult. Hence, knowledge of the thermal behaviour and associated

85   reactions affecting oil sands reservoirs during CSS has significant implications for successful

86   hydrocarbon recovery.

87   Laboratory experiments provide a good way to investigate the behaviour of oil sands

88   during steaming. Those by Kirk et al. (1987) are among the earliest studies of Clearwater oil sands

89   during steaming processes. Their samples were obtained from the Husky Oil Tucker Lake pilot site

90   in Athabasca area. Zhou et al. (1993, 1994, 1995) conducted a series of autoclave experiments at

91   250°C on Clearwater oil sands from Cold Lake area with a focus on the hydrothermal stability of

92   clays minerals, especially berthierine, which is among the most common clay minerals in the

93   Clearwater Formation.

94   In field tests, Longstaffe (1994) and McKay and Longstaffe (2013) demonstrated

95   the occurrence of oxygen- and hydrogen-isotope exchange between the injection fluids

96   and clay minerals during CSS of Clearwater Formation reservoirs. The change in oxygen-

97   and hydrogen-isotope compositions between pre- and post-steam clay minerals provides

98   insight into the extent of interaction between clay minerals and steam/steam condensate.

99   In the present study, pre- and post-steam clay minerals and solutions from autoclave tests

100   of Alberta Clearwater oil sands performed by Zhou et al. (1994) were analyzed for their

101   stable isotope compositions. The objectives were: (1) to determine the changes in the

102   oxygen- and hydrogen-isotope compositions of the clay minerals and solutions during

103   these experiments, (2) to understand the nature and extent of isotopic exchange between

104   the solutions and the clay minerals, and (3) to test whether isotopic data for post-steam

105   clay minerals record temperatures achieved by CSS. Such temperature estimates could

106   help to evaluate the distribution of steam/steam condensate within oil-sands reservoirs,

107   and hence judge the effectiveness of the CSS process.

108

109   **2. Materials and Methods**

110   *2.1. Materials*

111   Berthierine can comprise up to 80–90 % of the clay fraction in some sections of the

112   Clearwater Formation in the study area (Dean and Nahnybida, 1985; Longstaffe, 1994;

113   Hornibrook and Longstaffe, 1996; McKay and Longstaffe, 1997). Berthierine is iron-rich,

114   0.7 nm-layer silicate that typically envelops framework grains of Clearwater oil sands (Figs.

115   2a and 2b). Given its grain-coating and pore-lining nature, berthierine may preferentially

116   react with injection fluids during CCS and thus affect reservoir quality. Zhou et al. (1993,

117   1995) initially completed autoclave experiments to study the thermal stability of

118   berthierine using pure separates. Zhou et al. (1994) then undertook additional autoclave

119   experiments that better approximated the full fines mineralogy of these oil sands. They

120   conducted parallel autoclave experiments that utilized bulk sands, on one hand, and the

121   full assemblage of <2 μm phases isolated from the bulk sands, on the other hand. The <2

122   μm size-fraction from the bulk sands was dominated by berthierine. The current study

123   examined the <2 μm solids and associated solutions collected before (pre-run) and after

124   (post-run) these experiments. The oil sand samples used in the autoclave experiments

125   were obtained from the Imperial Oil Limited Cold Lake leases and are identified as ZB5

126   (Cold Lake 4-23-65 4W4 at 439.0 m) and ZB6 (Cold Lake 6-21-64 4W4 at 439.7 m). The

127   procedures used to isolate the <2 μm size-fraction are summarized in the Supplementary

128   Materials (Text S1).

129

130   *2.2. X-ray diffraction (XRD) analysis*

131   The mineralogy of the <2 μm solids used in the autoclave experiments was

132   determined by powder XRD analysis. Several pre-treatments were applied to the <2 μm

133   clay fraction to facilitate its identification. Treatments included Ca-saturation followed by

134   XRD analysis of oriented samples at (i) 54 % relative humidity (RH) and then (ii) after

135   vapour saturation with ethylene glycol, and K-saturation followed by XRD analysis of

136   oriented samples at (iii) 0% RH and then (iv) 54% RH, followed by heating to (v) 300 °C and

137   then (vi) 550 °C (Ignasiak et al., 1983). The relative mineral abundances of solids were

138   estimated based on background-subtracted, form-factor corrected, and normalized (001)

139   peak intensities (after Biscaye, 1965). The dioctahedral versus trioctahedral nature of the

140   clay phases was determined by measurement of the 06 band diffraction of randomly

141   oriented <2 μm size-fractions. XRD patterns for the <2 μm size-fractions of pre-run and

142   post-run solids are provided in the Supplementary Materials (Figs. S1-S10; from Zhou et

143   al., 1994).

144

a)

75mm

b)

6mm

c)

Sme

Anl

75mm

d)

Sme

29.5mm

145
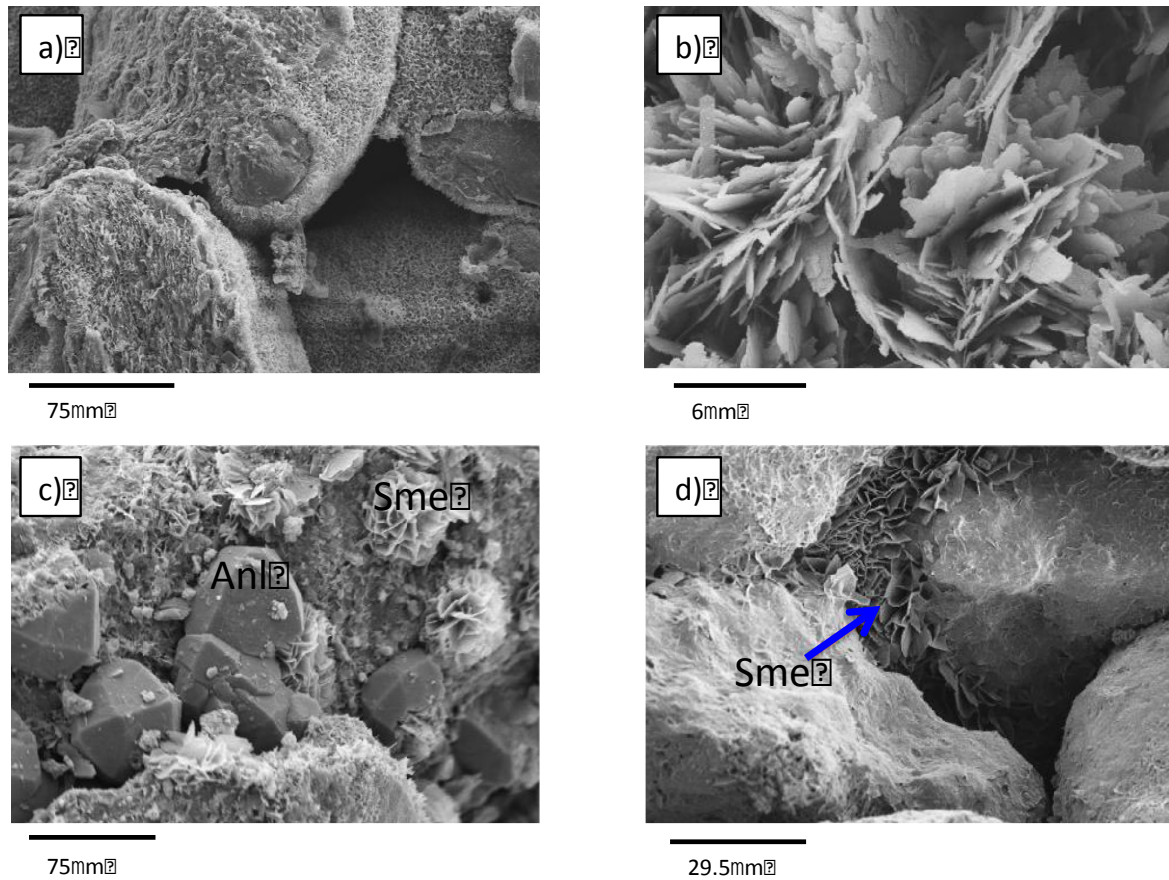
Fig. 2. Scanning electron microscope (SEM) images of bulk sands: (a) Berthierine coating on sand grains; (b) Berthierine blades; (c) Euhedral analcime (Anl) balls and smectite (Sme) formed during autoclave tests; (d) Smectite (Sme) formed in the pore space of sands during autoclave tests.

150

2.3. Chemical analysis of clay minerals

152   The chemical compositions of the clay mineral samples used in the present study

153   are listed in Zhou et al. (1994) and were obtained using the analytical electron microscope

154   (AEM) and the electron microprobe (EMP). The AEM analyses were performed at the

155   Electron Microscope Laboratory, the University of Michigan at Ann Arbor. The clays were

156   embedded in epoxy and a micro-thin section then cut after the epoxy hardened. These

157   thin sections were then ion-milled to produce ultra-thin edges on which AEM analysis was

158   performed. The EMP analyses were performed at Electron Microprobe Laboratory,

159   University of Alberta. A film of pure clay mineral separates was deposited onto a ceramic

160   disc, which was then air-dried and then oven-dried before being coated with carbon prior

161   to EMP analysis. Zhou et al.'s (1994) results, reconstituted into the form needed to

162   calculate oxygen-isotope clay-water geothermometers following Savin and Lee (1988), are

163   provided in the Supplementary Materials (Tables S1, S2 and S3).

164

165   *2.4. Stable isotope analysis*

166   The pre- and post-run <2 μm solids and solutions were analyzed for their oxygen- and

167   hydrogen-isotope compositions, and the results are reported in the usual δ-notation relative to

168   Vienna Standard Mean Ocean Water (VSMOW; Coplen, 1994). Prior to isotope analysis, samples

169   were heated at 150°C under vacuum overnight to remove adsorbed water. Structural oxygen was

170   then extracted from the samples using the BrF_5 method (Clayton and Mayeda, 1963). This oxygen

171   was then converted to CO_2 through reaction with hot graphite and the resulting CO_2 was analyzed

172   using a Micromass Optima dual-inlet isotope-ratio-mass-spectrometer (IRMS). Hydrogen-isotope

173   analyses were performed following the uranium technique and heating methods of Bigeleisen et

174   al. (1952), as modified by Kyser and O'Neil (1984).   Reproducibility was better than ± 0.2 ‰ for

175   oxygen isotopes and ± 2 ‰ for hydrogen isotopes. Standard laboratory quartz gave an average

176   measured $\delta^{18}O$ of +11.5 ± 0.1 ‰, which compares well with its accepted value (+11.5 ‰). Clay

177   standard KGa-1 kaolinite produced an average measured δ^2H of −57 ± 1 ‰, which compares well

178   with its accepted value (−57 ‰).

179   The oxygen- and hydrogen-isotope compositions of solutions were analyzed using the

180   methods of Epstein and Mayeda (1953) and Coleman et al. (1982), respectively. Two millilitres of

181   water sample were equilibrated with CO_2 at 25°C overnight for oxygen-isotope analysis. Hydrogen

182   gas for isotopic analysis was produced by reducing (under vacuum) 2 μl of water with metallic zinc

183   at 500°C for 20 min. Reproducibility was normally better than ± 0.1 ‰ for δ^{18}O and ± 2 ‰ for δ^2H.

184   Laboratory water standards calibrated to VSMOW and SLAP were accurate to within ± 2 ‰ for δ^2H

185   and ± 0.1 ‰ for δ^{18}O.

186

187   **3. Brief Description Of Autoclave Tests**

188   As reported in detail by Zhou et al. (1994), the autoclaves were loaded with 0.25 grams of

189   <2 μm solids (from ZB5 or ZB6) and 100 ml of one of four types of solution having different pH and

190   chemistry (Table 1). The samples were then sealed and heated at 250°C for 1008 hours, which are

191   a temperature and time typical of CSS. The results indicated that berthierine largely disappeared

192   during the hydrothermal reactions. In acidic solutions, Fe-chlorite was the major reaction product.

193   In neutral to alkaline solutions, the principal products replacing berthierine were swelling clays,

194   with minor amounts of analcime and in one case, chlorite (Table 2; Figs. 2c and 2d). The swelling

195   clay produced was mainly Fe-rich, tri-octahedral Fe-saponite in neutral solutions, and mixed-layer

196   chlorite-smectite in alkaline solutions. The reaction of berthierine to smectite plus analcime in

197   alkaline solution at 250°C was described by Zhou et al. (1993, 1994, 1995) as:

198   3 Berthierine + 6 Quartz + 3.3 H_2O +2.6 Na^+

199   = 2 Smectite + 2 Analcime + 2.6 H^+ [1]

200

4. Results

202   The stable isotope results for pre- and post-run solutions are presented in Table 3. There

203 were only small differences between the stable isotope compositions of the pre- and post-run

204 solutions. Pre-run solution $\delta^{18}O$ ranges from −19.8 to −17.2 ‰ and δ^2H from −154 to −146 ‰,

205 whereas post-run solution $\delta^{18}O$ ranges from −19.3 to −18.5 ‰ and δ^2H from −154 to −147 ‰.

206   In contrast, the pre- versus post-run <2 μm solids exhibit very different ranges of stable

207 isotope compositions (Table 3). Pre-run solids have $\delta^{18}O$ ranging from +9.5 to +12.9 ‰ and δ^2H

208 from −114 to −113 ‰. Such isotopic compositions are typical of berthierine-rich clay mixtures

209 from the Clearwater Formation (Hornibrook and Longstaffe, 1996). Post-run solid $\delta^{18}O$ and δ^2H

210 show a systematic decrease. For ZB5C solids, $\delta^{18}O$ ranges from −2.9 to +2.1 ‰ and δ^2H from −147

211 to −128 ‰; For ZB6C solids, $\delta^{18}O$ ranges from −4.7 to −0.6 ‰ and δ^2H from −139 to −129 ‰.

Table 1 Materials and conditions for autoclave tests

Sample ID	Size Fraction	Solution Composition	Temperature (°C)	Duration (weeks)	Pre-run pH 25 °C	Post-run pH* 25 °C	Post-run pH* 250 °C
ZB5C1	< 2 mm	0.1 M NaHCO$_3$ 2.5 Bar pCO$_2$	250	6	8.98	6.76	6.83
ZB5C2	< 2 mm	0.1 M NaHCO$_3$ 0.08 M NaOH	250	6	10.84	10.55	7.85
ZB5C3	< 2 mm	0.03 M Na2SiO$_3$ 0.1 M NaCl	250	6	12.21	12.05	9.55
ZB5C4	< 2 mm	0.01 M HCl	250	6	2.06	3.56	3.57
ZB6C1	< 2 mm	0.1 M NaHCO$_3$ 2.5 Bar pCO$_2$	250	6	8.44	6.42	6.42
ZB6C2	< 2 mm	0.1 M NaHCO$_3$ 0.08 M NaOH	250	6	10.48	10.34	7.35
ZB6C3	< 2 mm	0.03 M Na2SiO$_3$ 0.1 M NaCl	250	6	12.27	12.12	9.54
ZB6C4	< 2 mm	0.01 M HCl	250	6	2.12	3.38	4.59

212   *   pH at elevated temperature is calculated using SOLMINEQ.88 (Kharaka et al., 1988; Zhou et al., 1995)

213

214

Table 2 Normalized X-ray diffraction peak intensities of <2 mm fraction of pre- and post-run solids (wt%)*

Sample ID	Smectite	C-S**	I-S**	Chlorite	Illite	Berthierine	Analcime	Quartz	Albite
ZB5-prerun		14	27		1	53		4	2
ZB5C1		45		6		25	14	8	3
ZB5C2	95					1	1	3	
ZB5C3	83						10	2	5
ZB5C4				68	2			22	8
ZB6-Prerun		4				94		1	1
ZB6C1		11				88		0	0
ZB6C2	99					1			
ZB6C3	81						8	4	8
ZB6C4				95				5	

*   The abundances of clay minerals were obtained using the intensities of the (001) diffractions from Ca-glycolated (1.7 nm, 1.0 nm and 0.7 nm clays) and K-550 °C (1.4 nm clay) samples; All the individual values are rounded up to the closest 1 %.

215   ** C-S and I-S represent mixed-layer chlorite-smectite and illite-smectite, respectively.

216

Table 3 Stable isotope compositions of pre-and post-run solids and solutions*

Solutions								Solids		
	Pre-run			Post-run						
Solution ID	d ^{18}O	d ^{2}H	n*	d ^{18}O	n*	d ^{2}H	n*	Sample ID	d ^{18}O	d ^{2}H
	(‰, VSMOW)	(‰, VSMOW)		(‰, VSMOW)		(‰, VSMOW)			(‰, VSMOW)	(‰, VSMOW)
								ZB5-prerun	+12.9	−114
ZB5C1	−19.6	−152	1	−18.5	4	−149	3	ZB5C1	−1.0	−147
ZB5C2	−18.2	−151	2	−18.6	1	−149	1	ZB5C2	−0.5	−128
ZB5C3	−19.0	−149	1	−18.7	3	−149	1	ZB5C3	−2.9	N/A**
ZB5C4	−19.4	−148	2	−18.7	3	−148	1	ZB5C4	+2.0	−134
								ZB6-prerun	+9.5	−113
ZB6C1	−19.8	−154	1	−19.1	1	−153	1	ZB6C1	−0.7	−129
ZB6C2	−17.2	−146	2	−19.0	1	−147	1	ZB6C2	−4.7	−137
ZB6C3	−19.4	−152	1	−19.3	1	−154	1	ZB6C3	−3.9	−139
ZB6C4	−19.8	−154	2	−19.3	3	−153	1	ZB6C4	−0.6	N/A**

* Isotope analyses were performed shortly after the autoclave experiments were concluded; d-value reported is an average of n analyses; reproducibility was ± 1 ‰ for d2H and ± 0.2 ‰ for d18O.
** N/A=not analysed

217

218

219 **5. Discussion**

220 *5.1. Stable isotopes in solutions*

221   The absence of significant differences between the δ^{18}O and δ^{2}H of pre-and post-run

222 solutions shows that the solutions were isotopically "conservative" during the experiments. This

223 behaviour reflects the high solution/mineral ratio used in the experiments; for 100 ml solution and

224 0.25 grams of solids, the water/solid (molar) ratio is ~4000-5000:1 for hydrogen and ~800:1 for

225 oxygen. At such ratios, interaction between the solutions and solids would strongly affect the δ-

226 values of the solids but have little effect on the solutions.

227   During CSS, the water/mineral ratio for both oxygen and hydrogen may not be as high as

228 that in the autoclave experiments, and the factors affecting the resulting isotope compositions of

229 injected water are much more complex (McKay and Longstaffe, 2013). In addition to water-rock

230 interaction, interaction between steam and hydrocarbons can cause changes in the stable isotope

14

231 compositions of the production waters, especially for hydrogen (McKay and Longstaffe, 2013).

232 Such interaction could lead to lower than expected δ^2H for the co-existing clay minerals

233 (Sheppard, 1986; Fallick, 1993; McKay and Longstaffe, 2013). Formation water originally present

234 in units associated with the reservoir sands may also contribute to the final isotopic compositions

235 of fluids produced during CSS. As such, the isotopic behaviour of solutions measured during the

236 autoclave experiments may not be completely analogous to that of produced waters during CSS.

237 That said, McKay and Longstaffe (2013) reported very little difference in δ^{18}O between fresh

238 boiler-feed water and recycled water produced during CSS projects that were exploiting

239 berthierine-rich, Cold Lake oil sands.

240

241 *5.2. Isotope exchange between solids and solutions*

242   In addition to the mineral reactions (e.g. equation [1]) described by Zhou et al. (1993,

243 1994, 1995), oxygen- and hydrogen-isotope exchange occurred between the solids and solutions

244 during the autoclave experiments. Given the high water/solid ratios of the autoclave experiments,

245 the isotopic compositions of the pre-run solids would be expected to have shifted towards values

246 calculated for equilibrium with the solutions at 250°C. The extent of this process can be described

247 as the percentage of exchange (Yeh and Epstein, 1978):

248   Percentage Exchange = $[(\delta_M - \delta_{Pre})/(\delta_{eq} - \delta_{Pre})]$ x 100   [2]

249 where δ_M represents the measured δ^{18}O or δ^2H of the post-run solids, δ_{Pre} represents the δ^{18}O or

250 δ^2H of the pre-run solids, and δ_{eq} refers to the calculated δ^{18}O or δ^2H of the solid in isotopic

251 equilibrium with the solutions at 250°C.

252   The solids used in the autoclave tests consist of multiple phases (Table 2) and thus their

253   stable isotope compositions are the combination of the contributions from all phases present:

254     $\delta_{Solid} = \Sigma\ X_i\ \delta_i$ [3]

255   where X_i refers to the mole fraction of phase i for oxygen or hydrogen, and δ_i refers to oxygen- or

256   hydrogen-isotope compositions of phase i in the solids.

257   The equilibrium stable isotope compositions expected for the solids at 250°C can be

258   estimated using mineral-water oxygen- and hydrogen-isotope fractionation factors. The average

259   stable isotope compositions of the solutions, −19.0 ‰ for $\delta^{18}O$ and −150 ‰ for $\delta^{2}H$, were used in

260   all calculations that follow. The oxygen-isotope clay mineral-water geothermometers were

261   calculated according to the bond-strength method of Savin and Lee (1988), using the average

262   chemical compositions of these clay minerals reported in Tables S1, S2 and S3:

263     $10^{3}ln\alpha_{berthierine-water} = 4.801\ (10^{3})T^{-1} + 2.653\ (10^{6})T^{-2}$

264             $- 0.470\ (10^{9})T^{-3} + 0.042\ (10^{12})T^{-4} - 13.57$ [4]

265     $10^{3}ln\alpha_{saponite-water} =\ 6.021T^{-1} + 6.084\ (10^{6})T^{-2}$

266      $- 0.087\ (10^{9})T^{-3} + 0.078\ (10^{12})T^{-4} - 2.30$ [5]

267     $10^{3}ln\alpha_{chlorite-water} = 5.542\ (10^{3})T^{-1} + 2.323\ (10^{6})T^{-2}$

268             $- 0.392\ (10^{9})T^{-3} + 0.035\ (10^{12})T^{-4} - 13.68$ [6]

269   Chemical data for illite in the solids were not available. Instead, the equation of Sheppard and Gilg

270   (1996) has been used here,

271    $10^3 \ln\alpha_{\text{illite-water}} = 2.39 \ (10^6)T^{-2} - 3.76$ [7]

272 Likewise, in the absence of chemical data, equation 5 was applied to the mixed-layer chlorite-

273 smectite.

274   The following oxygen-isotope mineral-water geothermometers have been used for quartz,

275 albite, and analcime:

276    $10^3 \ln\alpha_{\text{quartz-water}} = 3.34 \ (10^6)T^{-2} - 3.31$ (Matsuhisa et al., 1979) [8]

277    $10^3 \ln\alpha_{\text{albite-water}} = 2.39 \ (10^6)T^{-2} - 2.51$ (Matsuhisa et al., 1979) [9]

278    $10^3 \ln\alpha_{\text{analcime-water}} = 2.78 \ (10^6)T^{-2} - 2.89$

279   (Karlsson and Clayton, 1990)   [10]

280   Only clay minerals were considered in the calculation of hydrogen-isotope compositions in

281 equilibrium with the solutions at 250°C, as most other phases present do not contain significant

282 hydrogen in their structure. Analcime does contain channel water, which is very difficult to

283 analyze, and some fraction of this water can exchange with the atmosphere under ambient

284 conditions in the laboratory. However, appropriate pre-treatment removes most channel water

285 from analcime prior to analysis. Hydrogen-isotope fractionation factors between clay minerals and

286 waters are less well-known than for oxygen (Savin and Lee, 1988; Sheppard and Gilg, 1996). The

287 following hydrogen-isotope fractionation factors at 250°C were used for illite, saponite, chlorite,

288 and berthierine, respectively:

289    $10^3 \ln\alpha_{\text{illite-water}} = -25$ (O'Neil and Kharaka, 1976)   [12]

290    $10^3 \ln\alpha_{\text{saponite-water}} = -30$ (Kulla, 1979)   [13]

291   $$10^3 \ln\alpha_{chlorite\&berthierine-water} = -40 \quad \text{(Marumo et al., 1980)} \quad \text{[14]}$$

292   Equation 13 was also used to calculate the equilibrium δ-values for all other swelling clays present

293   in the solids.

294

Table 4 Percentage of oxygen- and hydrogen-isotope exchange between the solids and solutions at 250 °C

Sample ID	$d^{18}O$			d^2H		
	Equilibrium value (‰, VSMOW)	Measured (‰, VSMOW)	Percentage exchange (%)	Equilibrium value (‰, VSMOW)	Measured (‰, VSMOW)	Percentage exchange (%)
ZB5C1	−12.8	−1.0	54	−180	−147	50
ZB5C2	−14.3	−0.5	49	−175	−128	23
ZB5C3	−14.0	−2.9	58	−175	N/A*	N/A*
ZB5C4	−11.5	+2.1	44	−181	−134	30
ZB6C1	−16.2	−0.7	40	−183	−129	23
ZB6C2	−15.7	−4.7	56	−175	−137	39
ZB6C3	−13.6	−3.9	58	−175	−139	41
ZB6C4	−13.6	−0.6	44	−183	N/A*	N/A*

295   * N/A = not available

296

297   Table 4 and Fig. 3 compare the calculated oxygen- and hydrogen-isotope compositions of

298   the solids in isotopic equilibrium with the experimental solutions at 250°C, according to the

299   equations presented above, with the measured results. The large difference between the

300   calculated equilibrium and measured compositions of the post-run solids shows that isotopic

301   equilibrium with the solutions was not achieved during these experiments. The calculated

302   percentage of oxygen-isotope exchange (40 to 58%) for the clay minerals is higher on average than

303   that obtained for hydrogen isotopes (23 to 50%).

304

305
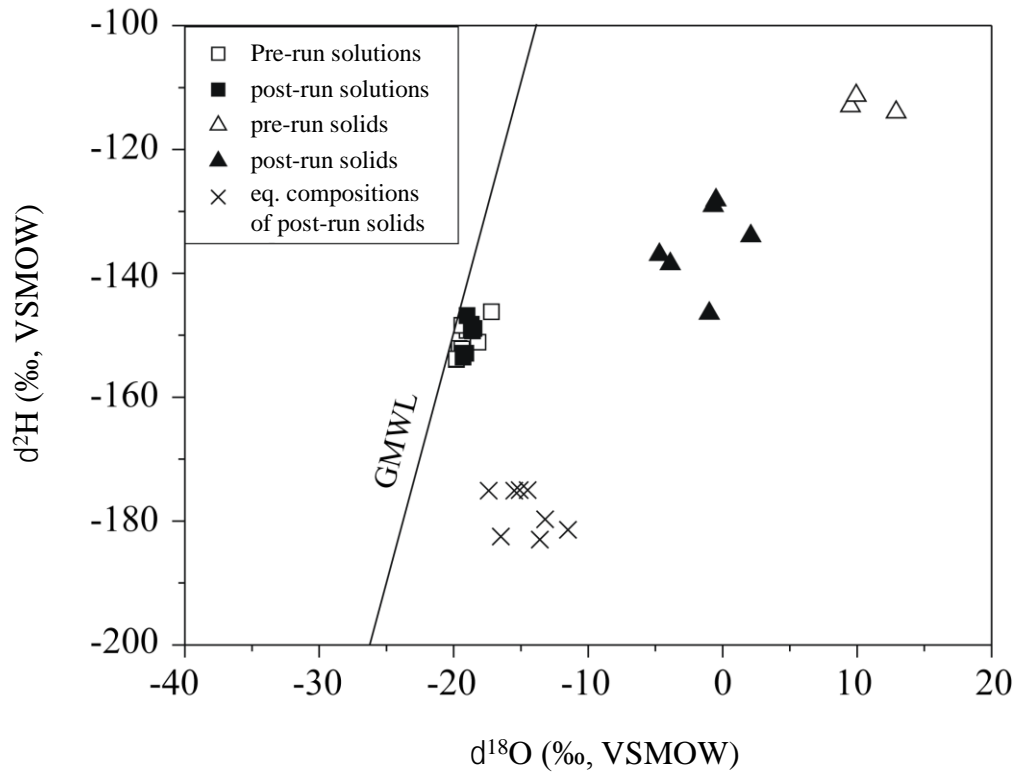
Fig. 3. δ^2H versus $\delta^{18}O$ of pre- and post-run solutions and solids from the autoclave experiments.

Post-run equilibrium isotopic compositions for the solids at 250 ˚C were calculated using the

isotope geothermometers and fractionation factors discussed in the text. The initial injection

water was drawn from local resources and plots close to the Global Meteoric Water Line (GMWL)

of Craig (1961) at compositions typical of this region. Isotope equilibrium compositions of post-run

solids were calculated based on the fractionation factors discussed in the text. eq. = equilibrium.

312

The higher percentage of exchange for oxygen than hydrogen was not anticipated. Several

studies (O'Neil and Kharaka, 1976; Yeh and Epstein, 1978; Longstaffe and Ayalon, 1990; Kyser and

Kerrich, 1991) have shown that hydrogen-isotope exchange between clay minerals and water is

faster than for oxygen at low temperatures. Significant hydrogen-isotope exchange can occur at

temperatures below 100 °C, unaccompanied by major oxygen-isotope exchange (Yeh and Epstein,

1978; Longstaffe and Ayalon, 1990). It has been postulated that the replacement of H⁺ rather than

(OH)⁻ controls hydrogen-isotope exchange at low temperatures but the replacement of (OH)⁻ can

320   become much more important in controlling hydrogen-isotope exchange with water at higher

321   temperatures (Longstaffe, 2000). Therefore, it was initially expected that hydrogen isotopes

322   would have been more, or at least equally, affected by isotopic exchange during the mineral-

323   solution reactions.

324   We have considered whether the lower calculated amount of hydrogen-isotope exchange

325   between the clay minerals and the solutions arose because of an inaccurate fractionation factor

326   for smectite, berthierine or chlorite. Several studies have shown that hydrogen-isotope

327   fractionation factors between water and clay minerals having complicated chemical compositions

328   are not overly sensitive to temperature (Marumo et al., 1995; Sheppard and Gilg, 1996; Ziegler

329   and Longstaffe, 2000). In natural, hydrothermal chlorite-water systems, for example, Marumo et

330   al. (1995) found that the hydrogen-isotope fractionation varied more as a function of iron content

331   in octahedral sites, and Sheppard and Gilg (1996) showed similar behaviour for smectite at low

332   temperatures. Based on the chemical data for chlorite from Marumo et al. (1980, 1995), Ziegler

333   and Longstaffe (2000) reported an equation for the hydrogen-isotope fractionation between

334   chlorite and water as follows:

335        $10^3 \ln\alpha_{chlorite-water} = 1.3521 - 93.165 * (Fe/(Fe + Mg))$ [15]

336   where Fe is the total iron content. Analysis of the Clearwater clays indicated a very high Fe-

337   content in the octahedral sites (Tables S1, S2 and S3; specifically, for berthierine specifically, see

338   also Hornibrook and Longstaffe, 1996). If equation [15] is used for calculations instead of equation

339   [14], we obtain a clay-water fractionation factor of −76 to −60‰, which produces even lower

340   equilibrium hydrogen-isotope compositions for chlorite and berthierine, and thus an even lower

341   calculated percentage of isotopic exchange. A similar argument can be made for the Fe-rich

342   saponite reaction product, for which larger clay-water H-isotope fractionations can also be

20

343   anticipated (Sheppard and Gilg, 1996). Hence, a different mechanism is needed to explain these

344   results.

345

346   *5.3. Structure inheritance in clay minerals*

347   A possible explanation for the measured oxygen- and hydrogen-isotope compositions of

348   the autoclave reaction products is that the post-run clays (smectite, chlorite-smectite and chlorite)

349   inherited part of their oxygen and hydrogen from precursor berthierine. The idea that minerals

350   might inherit structural components from precursors has been proposed previously (e.g.,

351   Robertson and Eggleton, 1991; Bird et al., 1994). Robertson and Eggleton (1991) examined

352   kaolinite and halloysite from weathered granites using SEM and TEM, and found that one

353   tetrahedral sheet in muscovite appeared to have been removed to convert the remaining 1:1 layer

354   structure to a 0.7 nm kaolinite. Bird et al. (1994) investigated the gibbsite-water oxygen-isotope

355   fractionation factor ($\alpha_{gibbsite-water}$) using both synthesis experiments and natural samples. They

356   hypothesized that the higher apparent $\alpha_{gibbsite-water}$ commonly obtained for natural gibbsite

357   samples resulted from inheritance of tetrahedral sheet apical oxygens during desilication of

358   kaolinite. The kaolinite non-hydroxyl sheet oxygen is known to be enriched in ^{18}O relative to

359   hydroxyl oxygen by ~27 ‰ at surface temperatures (Girard and Savin, 1996).

360   Here we propose that isotopic inheritance from pre-run berthierine (1:1 layer) can explain

361   the incomplete isotopic exchange measured for the post-run clay minerals, using smectite (2:1

362   layer) as an example. If smectite formed solely by precipitation from the solutions fed by

363   dissolution of pre-run solids, all oxygen and hydrogen in the smectite should have acquired their

364   isotopic compositions from the solutions. In this scenario, the stable isotope compositions of the

365   post-run smectite should be close to the calculated values illustrated in Fig. 3, presuming that

366   isotopic equilibration occurred during clay neoformation. Instead, the percentage of oxygen-

367   isotope exchange observed for post-run smectite ranges from 49-58 % (avg. 55 %) and is lower still

368   for hydrogen (23-41 %, avg. 34 %) (Table 4). These amounts are similar for the experiments in

369   which chlorite and/or chlorite-smectite were produced (oxygen, 40-54 %, avg. 46 %; hydrogen, 23-

370   50 %, avg. 34 %).

371   The hydrothermal smectite 2:1 layer structure could also be formed by precipitation of a

372   tetrahedral sheet ('silication') onto a pre-existing berthierine 1:1 layer. In the simplest case, only

373   ten out of twenty-four oxygen atoms in the smectite structure would originate from the solution,

374   some original hydroxyl groups in the precursor berthierine would be lost to facilitate docking of

375   the tetrahedral sheet to the precursor octahedral sheet, and no new hydrogen would be added

376   (Fig. 4). This would result in 42% oxygen-isotope exchange (ignoring complications from

377   intracrystalline oxygen-isotope fractionation in clay minerals; Girard and Savin, 1996) and 0%

378   hydrogen-isotope exchange.
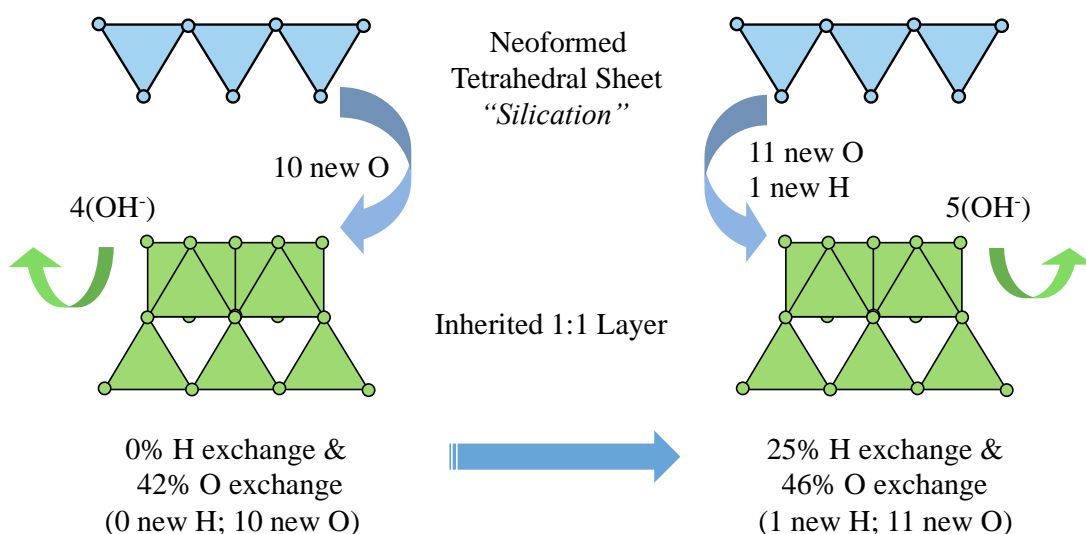
379

380   **Fig. 4**. A model for the formation of smectite during the autoclave tests. A neoformed tetrahedral

381   sheet is accreted to the 1:1 layer of berthierine to create the 2:1 layer structure of smectite that

382   inherits much of the original structure of the berthierine. Left: Four (4) hydroxyl groups are

383   removed from the berthierine's octahedral sheet to facilitate docking of neoformed tetrahedral

384   sheet with 10 new oxygens added to create the smectite. Right: Five (5) hydroxyl groups are

385   removed from the berthierine's octahedral sheet during smetite formation, resulting in 1 new

386   hydrogen (octahedral sheet) and 11 new oxygen in the structure (10 and 1 to the tetrahedral and

387   octahedral sheets, respectively. Note: the formula of smectite is calculated based on $O_{20}(OH)_4$.

388

389   The cation-hydroxyl bond (e.g., Al-OH) is weaker than the cation-oxygen bond (e.g., Al-O-

390   Si) and hence hydroxyl groups tend to be exchanged or replaced more readily than oxygen bonded

391   only to cations. If one out of four of the hydroxyl groups in the new smectite had originated from

392   the solutions, or isotopically exchanged with a precursor hydroxyl during the berthierine to

393   smectite transformation, the amounts of oxygen- and hydrogen-isotope exchange would increase

394   to 46% and 25%, respectively (Fig. 4). If two hydroxyl groups underwent such processes during

395   smectite formation, the amounts of oxygen- and hydrogen-isotope exchange would each reach

396   50%.

397   This conceptual model provides a mechanism to explain the amount of oxygen- and

398   hydrogen-isotope exchange measured for the post-run smectites (and the chlorite-smectite and

399   chlorite). The lack of an exact match between measured versus predicted percentages of isotopic

400   exchange points to the complexity that can accompany partial inheritance from a precursor 1:1

401   layer phase. Some of the mismatch may reflect a failure to account for intracrystalline oxygen-

402   isotope fractionation at hydrothermal temperatures during tetrahedral sheet neoformation and

403   hydroxyl group loss/exchange as the silica sheet is docked to the precursor 1:1 layer. Other

404   processes operating likely include proton exchange between the octahedral sheet hydrogen and

405   the solutions (e.g., Longstaffe and Ayalon, 1990), and anion exchange of original non-hydroxyl

406   oxygen, particularly when coordinated with Fe. Notwithstanding these caveats, the results of this

407   study suggest that inheritance from precursors should be considered when interpreting the

408   oxygen- and hydrogen-isotope compositions produced during clay mineral transformations at

409   hydrothermal temperatures over relatively short periods of time.

410   In this regard, we note that McKay and Longstaffe (2013) examined the stable isotope

411   compositions of clay minerals obtained directly from pre- and post-steam Clearwater oil sand

412   reservoirs in Alberta, Canada. They noticed a significant variation in δ^{18}O of post-steam smectite

413   formed in near-injector cores but no systematic shift in its δ^2H. To the possible explanations for

414   this unexpected behaviour offered by McKay and Longstaffe (2013), we can now add the

415   possibility of CSS-related smectite formation built upon precursor berthierine scaffolding, and the

416   isotopic inheritance that accompanies that mechanism of secondary 2:1 layer clay formation

417

418   **6. Conclusions**

419   The <2 μm clay minerals from Clearwater Formation oil sands of Alberta, Canada showed a

420   change in mineralogy from berthierine-dominated to smectite and / or chlorite-smectite and

421   chlorite-dominated assemblages following autoclave experiments conducted at 250 °C for 1008

422   hours. Following reaction with the low ^{18}O and low ^{2}H autoclave solutions at very high water/solid

423   ratios, there was a marked decrease in the δ^{18}O and δ^2H of the post-run products compared to the

424   starting solids. Neither oxygen- nor hydrogen-isotope equilibrium, however, was established

425   between the solids and the solutions. For all solids, the oxygen-isotope exchange (40 to 58 %; avg.

426   50 %) was generally higher than for hydrogen isotopes (23 to 50 %; avg. 34 %). This pattern is

427   attributed to formation of the reaction product clay minerals in part by structural and isotopic

428   inheritance from precursor 1:1 layer berthierine. Our results reinforce the importance of

429   considering isotopic and structural inheritance from precursor phases when interpreting isotopic

430   data, especially for transformations from one clay mineral to another. Isotopic inheritance from a

431   precursor phase will also limit the usefulness of the oxygen- and hydrogen-isotope compositions

432   of post-CSS clay minerals as an *in situ* recording of reservoir temperature and steam/steam-

433   condensate contact.

434

444

445   **References**

446

447   Alberta Energy, 2018. About Oil Sands: Facts and statistics.

448   http://www.energy.alberta.ca/OS/AOS/Pages/FAS.aspx.

449   Alvarez, J., Han, S., 2013. Current overview of cyclic steam injection process. J. Pet. Sci. Res. 2, 12.

450   Banerjee, D.K., 2012. Oil sands, heavy oil & bitumen: from recovery to refinery. PennWell Corp,

451   Tulsa, Okla.

452   Barrett, M.L., Mathias, R.W., 1992. Sediment alteration and fines migration in enhanced recovery

453   operations, Tertiary Heavy Oil Fields, California, in: SPE Formation Damage Control

454   Symposium. Society of Petroleum Engineers. https://doi.org/10.2118/23782-MS

455   Beattie, C.I., Boberg, T.C., McNab, G.S., 1991. Reservoir simulation of cyclic steam stimulation in

456   the Cold Lake oil sands. SPE Reservoir Eng. 6, 200-206. https://doi.org/10.2118/18752-PA

457   Bigeleisen, J., Perlman, M.L., Prosser, H.C., 1952. Conversion of hydrogenic materials to hydrogen

458   for isotopic analysis. Anal. Chem. 24, 1356–1357. https://doi.org/10.1021/ac60068a025

459   Bird, M.I., Longstaffe, F.J., Fyfe, W.S., Tazaki, K., Chivas, A.R., 1994. Oxygen-isotope fractionation in

460   gibbsite: Synthesis experiments versus natural samples. Geochim. Cosmochim. Acta 58,

461   5267–5277. https://doi.org/10.1016/0016-7037(94)90310-7

462   Chopra, S., Lines, L.R., Schmitt, D.R., Batzle, M.L., 2010. Heavy-oil reservoirs: Their characterization

463   and production, in: Chopra, S., Lines, L.R., Schmitt, D.R., Batzle, M.L. (Eds.), Heavy Oils:

464   Reservoir characterization and production monitoring, Society of Exploration

465   Geophysicists, pp. 1-69. https://doi.org/10.1190/1.9781560802235.ch1

466   Civan, F., 2016. Reservoir Formation Damage: Fundamentals, Modeling, Assessment,

467   and Mitigation, third ed. Elsevier, Amsterdam, Boston, Heidelberg, London, New York,

468   Oxford, Paris, San Diego, San Francisco, Singapore, Sydney and Tokyo.

469   Clayton, R.N., Mayeda, T.K., 1963. The use of bromine pentafluoride in the extraction of oxygen

470   from oxides and silicates for isotopic analysis. Geochim. Cosmochim. Acta 27, 43–52.

471   https://doi.org/10.1016/0016-7037(63)90071-1

472   Coleman, M.L., Shepherd, T.J., Durham, J.J., Rouse, J.E., Moore, G.R., 1982. Reduction of water

473   with zinc for hydrogen isotope analysis. Anal. Chem. 54, 993–995.

474   https://doi.org/10.1021/ac00243a035

475   Coplen, T.B., 1994. Reporting of stable hydrogen, carbon, and oxygen isotopic abundances

476   (Technical Report). Pure Appl. Chem. 66, 273–276.

477   https://doi.org/10.1351/pac199466020273

478   Craig, H., 1961. Standard for reporting concentrations of deuterium and oxygen-18 in natural

479   waters. Science 133, 1833. https://doi.org/10.1126/science.133.3467.1833

480   Dean, R.S., Nahnybida, C., 1985. Authigenic trioctahedral clay minerals coating Clearwater

481   Formation sand grains in Cold Lake, Alberta — Extended abstract. Appl. Clay Sci. 1, 237–

482   238. https://doi.org/10.1016/0169-1317(85)90577-0

483   Epstein, S., Mayeda, T., 1953. Variation of O^{18} content of waters from natural sources. Geochim.

484   Cosmochim. Acta 4, 213–224. https://doi.org/10.1016/0016-7037(53)90051-9

485   Fallick, A.E., 1993. Implications of linearly correlated oxygen and hydrogen isotopic compositions

486   for kaolinite and illite in the Magnus Sandstone, North Sea. Clays Clay Miner. 41, 184–190.

487   https://doi.org/10.1346/CCMN.1993.0410207

488   Giesy, J.P., Anderson, J.C., Wiseman, S.B., 2010. Alberta oil sands development. Proc. Natl. Acad.

489   Sci. 107, 951. https://doi.org/10.1073/pnas.0912880107

490 Girard, J.-P., Savin, S.M., 1996. Intracrystalline fractionation of oxygen isotopes between hydroxyl

491   and non-hydroxyl sites in kaolinite measured by thermal dehydroxylation and partial

492   fluorination. Geochim. Cosmochim. Acta 60, 469–487. https://doi.org/10.1016/0016-

493   7037(95)00421-1

494 Gray, D.H., Rex, R.W., 1966. Formation damage in sandstones caused by clay dispersion and

495   migration, in: Bailey, S.W. (Ed.), 14th National Conference on Clays and Clay Minerals.

496   Pergamon, pp. 355–366. https://doi.org/10.1016/B978-0-08-011908-3.50033-5

497 Hardy, R.G., Tucker, M.E., 1988. X-ray powder diffraction of sediments, in: Tucker, M.E. (Ed.),

498   Techniques in Sedimentology. Blackwell Scientific, Oxford, p. 394.

499 Hashemi, R., Nassar, N.N., Pereira Almao, P., 2014. Nanoparticle technology for heavy oil *in-situ*

500   upgrading and recovery enhancement: Opportunities and challenges. Appl. Energy 133,

501   374–387. https://doi.org/10.1016/j.apenergy.2014.07.069

502 Hornibrook, E.R.C., Longstaffe, F.J., 1996. Berthierine from the Lower Cretaceous Clearwater

503   Formation, Alberta, Canada. Clays Clay Miner. 44, 1–21.

504   https://doi.org/10.1346/CCMN.1996.0440101

505 Ignasiak, T.M., Kotlyar, L., Longstaffe, F.J., Strausz, O.P., Montgomery, D.S., 1983. Separation and

506   characterization of clay from Athabasca asphaltene. Fuel 62, 353–362.

507   https://doi.org/10.1016/0016-2361(83)90096-0

508 Jiang, Q., Thornton, B., Russel-Houston, J.R., Spence, S., 2010. Review of thermal recovery

509   technologies for the Clearwater and Lower Grand Rapids Formations in the Cold Lake area

510   in Alberta. J. Can. Pet. Technol. 49, 2-13. https://doi.org/10.2118/140118-PA

511   Karlsson, H.R., Clayton, R.N., 1990. Oxygen isotope fractionation between analcime and water: An

512   experimental study. Geochim. Cosmochim. Acta 54, 1359–1368.

513   https://doi.org/10.1016/0016-7037(90)90161-D

514   Kharaka, Y.K., Gunter, W.D., Aggarwal, P.K., Perkins, E.H., Debraal, J.D., 1988. SOLMINEQ.88; a

515   computer program for geochemical modeling of water-rock interactions (No. 88–4277).

516   U.S. Geological Survey. https://doi.org/10.3133/wri884227

517   Kirk, J.S., Bird, G.W., Longstaffe, F.J., 1987. Laboratory study of the effects of steam condensate

518   flooding in the Clearwater Formation; high temperature flow experiments. Bull. Can. Pet.

519   Geol. 35, 34–47.

520   Krueger, R.F., 1988. An overview of formation damage and well productivity in oilfield operations:

521   An Update. In SPE-17459-MS. Presented at the SPE California Regional Meeting, 23-25

522   March, 2018, Society of Petroleum Engineers, SPE. SPE-17459-MS.

523   https://doi.org/10.2118/17459-MS

524   Kulla, J.B., 1979. Oxygen and hydrogen isotope fractionation factors determined in experimental

525   clay-water system. Ph.D. thesis, University of Illinois at Urbana-Champaign, Urbana-

526   Champaign, Illinois, USA.

527   Kyser, T.K., Kerrich, R., 1991. Retrograde exchange of hydrogen isotopes between hydrous

528   minerals and water at low temperatures, in: Taylor, H.P., J.R. O'Neil, J.R., Kaplan, I.R.

529   (Eds.), Stable Isotope Geochemistry: A Tribute to Samuel Epstein, The Geochemical

530   Society, Special Publication 3, Washington, DC, USA, pp. 409-422.

531   Kyser, T.K., O'Neil, J.R., 1984. Hydrogen isotope systematics of submarine basalts. Geochim.

532   Cosmochim. Acta 48, 2123–2133. https://doi.org/10.1016/0016-7037(84)90392-2

533   Longstaffe, F.J., 1994. Stable isotopic constraints on sandstone diagenesis in the Western Canada

534   Sedimentary Basin, in: Parker, A., Sellwood, B.W. (Eds.), Quantitative Diagenesis: Recent

535   Developments and Applications to Reservoir Geology, NATO ASI (Series C: Mathematical

536   and Physics Sciences). Springer Netherlands, Dordrecht, pp. 223–274.

537   https://doi.org/10.1007/978-94-011-0189-9_7

538   Longstaffe, F.J., Ayalon, A., 1990. Hydrogen-isotope geochemistry of diagenetic clay minerals from

539   Cretaceous sandstones, Alberta, Canada: evidence for exchange. Appl. Geochem. 5, 657–

540   668. https://doi.org/10.1016/0883-2927(90)90063-B

541   Marumo, K., Longstaffe, F.J., Matsubaya, O., 1995. Stable isotope geochemistry of clay minerals

542   from fossil and active hydrothermal systems, southwestern Hokkaido, Japan. Geochim.

543   Cosmochim. Acta 59, 2545–2559. https://doi.org/10.1016/0016-7037(95)00149-2

544   Marumo, K., Nagasawa, K., Kuroda, Y., 1980. Mineralogy and hydrogen isotope geochemistry of

545   clay minerals in the Ohnuma geothermal area, northeastern Japan. Earth Planet. Sci. Lett.

546   47, 255–262. https://doi.org/10.1016/0012-821X(80)90041-2

547   Matsuhisa, Y., Goldsmith, J.R., Clayton, R.N., 1979. Oxygen isotopic fractionation in the system

548   quartz-albite-anorthite-water. Geochim. Cosmochim. Acta 43, 1131–1140.

549   https://doi.org/10.1016/0016-7037(79)90099-1

550   McCrimmon, G.G., 1996. Sedimentology and sequence stratigraphy of the lower Cretaceous

551   Clearwater Formation, Cold Lake, Alberta. M.Sc. thesis, University of Ottawa, Ottawa,

552   Canada.

553   McKay, J.L., Longstaffe, F.J., 2013. Tracking fluid movement during cyclic steam stimulation of

554   Clearwater Formation oil sands using stable isotope variations of clay minerals. Clays Clay

555   Miner. 61, 440–460. https://doi.org/10.1346/CCMN.2013.0610504

556   McKay, J.L., Longstaffe, F.J., 1997. Diagenesis of the lower Cretaceous Clearwater Formation,

557   Primrose area, Northeastern Alberta, in: Pemberton, S.G., James, D.P. (Eds.), Petroleum

558   Geology of the Cretaceous Mannville Group, Western Canada, Canadian Society of

559   Petroleum Geologists Memoir 18, Calgary, pp. 392-412.

560   Nadeau, P.H., 1998. An experimental study of the effects of diagenetic clay minerals on reservoir

561   sands. Clays Clay Miner. 46, 18–26. https://doi.org/10.1346/CCMN.1998.0460103

562   National Energy Board, 2000. Canada's oil sands: a supply and market outlook to 2015, an energy

563   market assessment. Calgary, Alberta.

564   http://publications.gc.ca/site/eng/9.647899/publication.html

565   O'Neil, J.R., Kharaka, Y.K., 1976. Hydrogen and oxygen isotope exchange reactions between clay

566   minerals and water. Geochim. Cosmochim. Acta 40, 241–246.

567   https://doi.org/10.1016/0016-7037(76)90181-2

568   Osacký, M., Geramian, M., Uhlík, P., Čaplovičová, M., Danková, Z., Pálková, H., Vítková, M.,

569   Kováčová, M., Ivey, D.G., Liu, Q., Etsell, T.H., 2017. Mineralogy and surface chemistry of

570   Alberta oil sands: Relevance to nonaqueous solvent bitumen extraction. Energy Fuels 31,

571   8910–8924. https://doi.org/10.1021/acs.energyfuels.7b00855

572   Robertson, I.D.M., Eggleton, R.A., 1991. Weathering of granitic muscovite to kaolinite and

573   halloysite and of plagioclase-derived kaolinite to halloysite. Clays Clay Miner. 39, 113–126.

574   https://doi.org/10.1346/CCMN.1991.0390201

575   Savin, S., Lee, M., 1988. Isotopic studies of phyllosilicates, in: Bailey, S.W. (Ed.), Hydrous

576   Phyllosilicates, Reviews in Mineralogy 19. Mineralogical Society of America, Washington,

577   D.C., U.S.A., pp. 189-223.

578   Sheng, J.J., 2013. Cyclic steam stimulation, in: Sheng, J.J (Ed.), Enhanced Oil Recovery Field Case

579   Studies. Elsevier, pp. 389–412. https://doi.org/10.1016/B978-0-12-386545-8.00016-6

580   Sheppard, S.M.F., 1986. Characterization and isotopic variations in natural waters, in: Valley, J.W.,

581   Taylor, H.P., O'Neil, J.R. (Eds.), Stable Isotopes in High Temperature Geological Processes,

582   Reviews in Mineralogy 16. Mineralogical Society of America, Washington, D. C., U.S.A., pp.

583   165–183.

584   Sheppard, S.M.F., Gilg, H.A., 1996. Stable isotope geochemistry of clay minerals. Clay Miner. 31, 1–

585   24. https://doi.org/10.1180/claymin.1996.031.1.01

586   Speight, J.G., 2016. Heavy oil and tar sand bitumen, in: Speight, J.G. (Ed.), Introduction to

587   Enhanced Recovery Methods for Heavy Oil and Tar Sands. Elsevier, pp. 3–48.

588   https://doi.org/10.1016/B978-0-12-849906-1.00001-1

589   Wightman, D.M., Rottenfusser, B., Kramers, J., Harrison, R., 1989. Geology of the Alberta oil sands

590   deposit, in: Hepler, G., Chu, H. (Eds.), AOSTRA Technical Handbook on Oil Sands, Bitumen

591   and Heavy Oils, AOSTRA Technical Publication Series #6. Alberta Oil Sands Technology and

592   Research Authority, Edmonton, Alberta, pp. 1–6.

593   Wilson, M.J., Wilson, L., Patey, I., 2014. The influence of individual clay minerals on formation

594   damage of reservoir sandstones: a critical review with some new insights. Clay Miner. 49,

595   147–164. https://doi.org/10.1180/claymin.2014.049.2.02

596   Yeh, H.-W., Epstein, S., 1978. Hydrogen isotope exchange between clay minerals and sea water.

597   Geochim. Cosmochim. Acta 42, 140–143. https://doi.org/10.1016/0016-7037(78)90224-7

598   Zhou, Z., Gunter, W.D., Kadatz, B., Cameron, S., 1995. Hydrothermal stability of the clay minerals

599   from the Clearwater reservoirs at Cold Lake, Alberta, in: Meyer, R.F. (Ed.), Fueling for a

600   Clean and Safe Environment, Proceedings of the 6th UNITAR International Conference on

601   Heavy Crude and Tar Sands, Feb. 12-17, 1995, Houston, Texas. United States Department

602   of Energy, Bartlesville, OK, USA, pp. 27–35.

603   Zhou, Z., Gunter, W.D., Kadatz, B., Cameron, S., 1993. Hydrothermal stability of the berthierine

604   from Cold Lake, Alberta (Part I). AOSTRA/ARC/CANMET Industry Research Program, Report

605   #9293-10.

606   Zhou, Z., Kadatz, B., Cameron, S., Gunter, W.D., Perkins, E.H., 1994. Hydrothermal stability of the

607   berthierine from Cold Lake, Alberta (Part II). AOSTRA/ARC/CANMET Industry Research

608   Program, Report #9394-8.

609   Ziegler, K., Longstaffe, F.J., 2000. Clay mineral authigenesis along a mid-continental scale fluid

610   conduit in Palaeozoic sedimentary rocks from southern Ontario, Canada. Clay Miner. 35,

611   239–239. https://doi.org/10.1180/000985500546620

620   Sheppard, S.M.F., 1986. Characterization and isotopic variations in natural waters, in: Valley, J.W.,

621   Taylor, H.P., O'Neil, J.R. (Eds.), Stable Isotopes in High Temperature Geological Processes,

622   Reviews in Mineralogy 16. Mineralogical Society of America, Washington, D. C., U.S.A., pp.

623   165–183.

624   Sheppard, S.M.F., Gilg, H.A., 1996. Stable isotope geochemistry of clay minerals. Clay Miner. 31, 1–

625   24. https://doi.org/10.1180/claymin.1996.031.1.01

626   Speight, J.G., 2016. Heavy oil and tar sand bitumen, in: Speight, J.G. (Ed.), Introduction to

627   Enhanced Recovery Methods for Heavy Oil and Tar Sands. Elsevier, pp. 3–48.

628   https://doi.org/10.1016/B978-0-12-849906-1.00001-1

629   Wightman, D.M., Rottenfusser, B., Kramers, J., Harrison, R., 1989. Geology of the Alberta oil sands

630   deposit, in: Hepler, G., Chu, H. (Eds.), AOSTRA Technical Handbook on Oil Sands, Bitumen

631   and Heavy Oils, AOSTRA Technical Publication Series #6. Alberta Oil Sands Technology and

632   Research Authority, Edmonton, Alberta, pp. 1–6.

633   Wilson, M.J., Wilson, L., Patey, I., 2014. The influence of individual clay minerals on formation

634   damage of reservoir sandstones: a critical review with some new insights. Clay Miner. 49,

635   147–164. https://doi.org/10.1180/claymin.2014.049.2.02

636   Yeh, H.-W., Epstein, S., 1978. Hydrogen isotope exchange between clay minerals and sea water.

637   Geochim. Cosmochim. Acta 42, 140–143. https://doi.org/10.1016/0016-7037(78)90224-7

638   Zhou, Z., Gunter, W.D., Kadatz, B., Cameron, S., 1995. Hydrothermal stability of the clay minerals

639   from the Clearwater reservoirs at Cold Lake, Alberta, in: Meyer, R.F. (Ed.), Fueling for a

640   Clean and Safe Environment, Proceedings of the 6th UNITAR International Conference on

641   Heavy Crude and Tar Sands, Feb. 12-17, 1995, Houston, Texas. United States Department

642   of Energy, Bartlesville, OK, USA, pp. 27–35.

643   Zhou, Z., Gunter, W.D., Kadatz, B., Cameron, S., 1993. Hydrothermal stability of the berthierine

644   from Cold Lake, Alberta (Part I). AOSTRA/ARC/CANMET Industry Research Program, Report

645   #9293-10.

646   Zhou, Z., Kadatz, B., Cameron, S., Gunter, W.D., Perkins, E.H., 1994. Hydrothermal stability of the

647   berthierine from Cold Lake, Alberta (Part II). AOSTRA/ARC/CANMET Industry Research

648   Program, Report #9394-8.

649   Ziegler, K., Longstaffe, F.J., 2000. Clay mineral authigenesis along a mid-continental scale fluid

650   conduit in Palaeozoic sedimentary rocks from southern Ontario, Canada. Clay Miner. 35,

651   239–239. https://doi.org/10.1180/000985500546620

Supplementary Materials

Supplementary Text S1. Separation of <2 μm Size-fraction

Bitumen was cold-extracted from the starting materials using methanol chloride (Zhou et al., 1994). For the <2 μm size-fraction, grain-coating berthierine (and other original clay phases) were released from grains by ultrasonication. The spherical equivalent to the <2 μm size-fraction was then obtained by dispersion and then column settling at room temperature according to Stokes Law (Hardy and Tucker, 1988; McKay and Longstaffe, 2013). Following dialysis with a NaCl solution and then deionized water to remove excess Na+, the <2 μm size-fraction was then freeze-dried.

References

Hardy, R.G., Tucker, M.E., 1988. X-ray powder diffraction of sediments, in: Tucker, M.E. (Ed.), Techniques in Sedimentology. Blackwell Scientific, Oxford, p. 394.

McKay, J.L., Longstaffe, F.J., 2013. Tracking fluid movement during cyclic steam stimulation of Clearwater Formation oil sands using stable isotope variations of clay minerals. Clays Clay Miner. 61, 440–460. https://doi.org/10.1346/CCMN.2013.0610504

Zhou, Z., Kadatz, B., Cameron, S., Gunter, W.D., Perkins, E.H., 1994. Hydrothermal stability of the berthierine from Cold Lake, Alberta (Part II). AOSTRA/ARC/CANMET Industry Research Program, Report #9394-8.
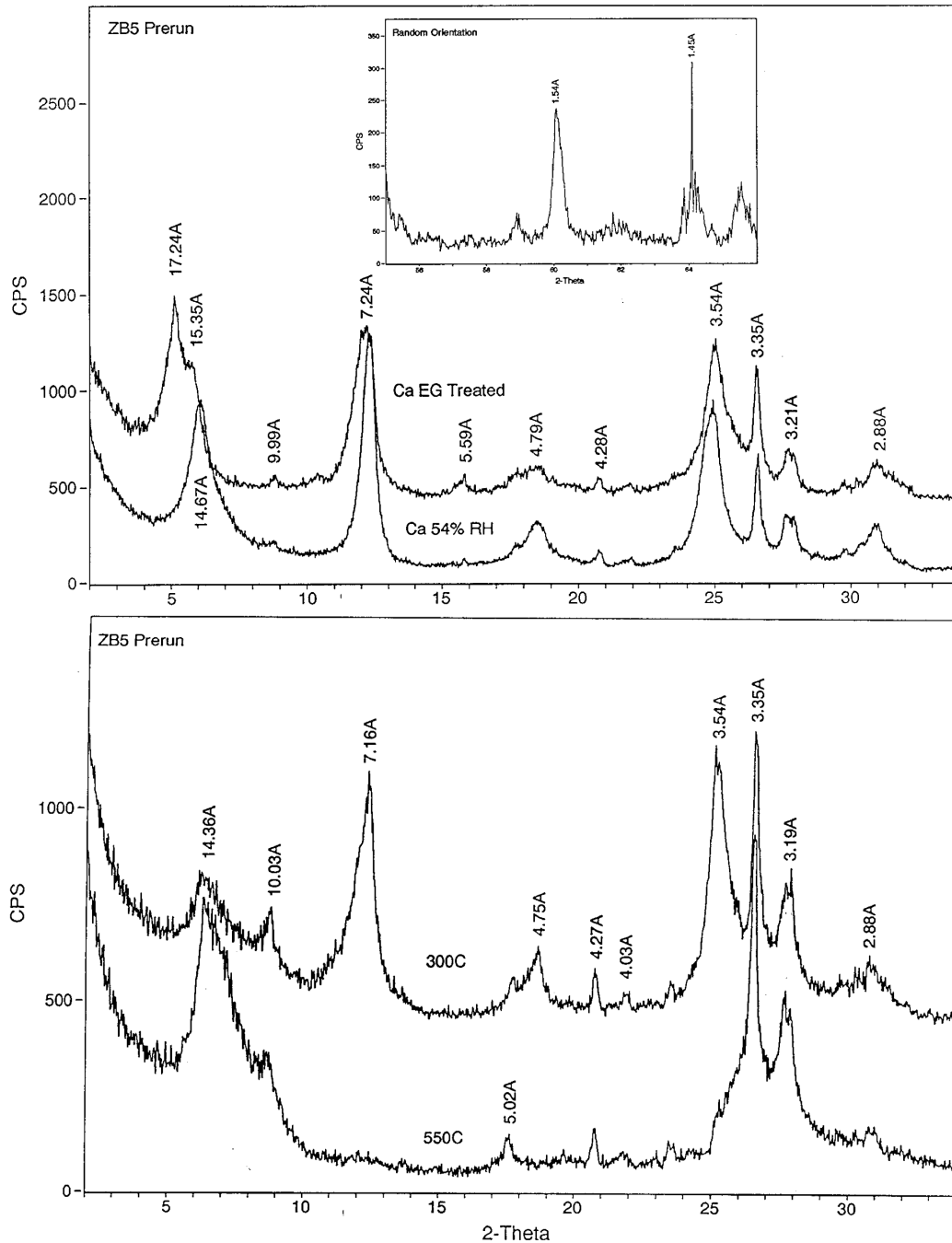
Fig. S1. XRD patterns of the <2 μm size-fraction of ZB5-prerun with different pre-treatment: Ca-saturation at 54% RH, vapour saturation with ethylene glycol (EG), and K-saturation followed by heating to 300°C and then 550°C (from Zhou et al., 1994). The 06 band diffraction pattern for randomly oriented samples is also illustrated together with the patterns for the preferred-oriented Ca-saturated samples.
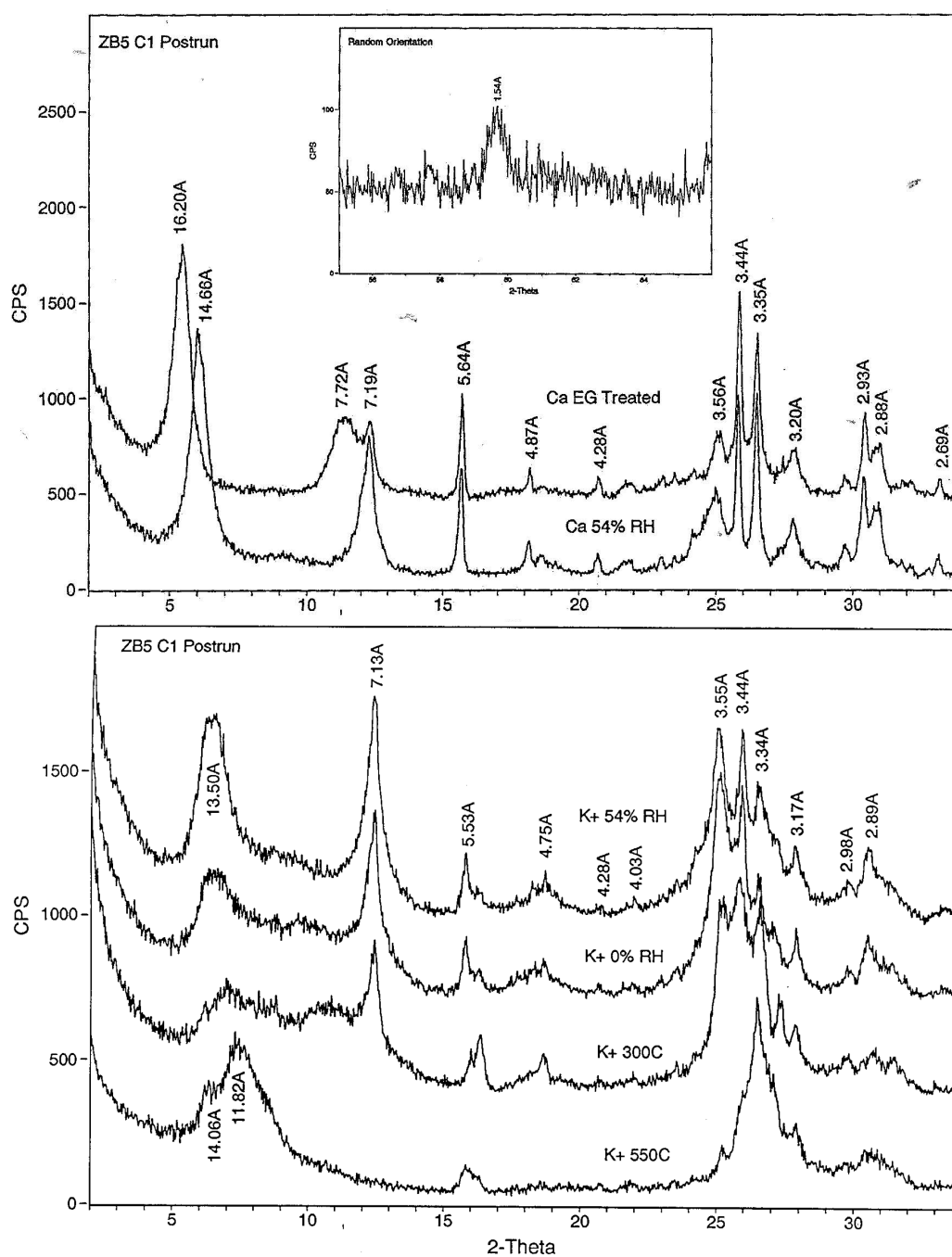
Fig. S2. XRD patterns of the <2 μm size-fraction of post-run solid ZB5C1 with different pre-treatment: Ca-saturation at 54% RH, vapour saturation with ethylene glycol (EG), and K-saturation at 0% RH and 54% RH, followed by heating to 300°C and then 550°C (from Zhou et al., 1994). The 06 band diffraction pattern for randomly oriented samples is also illustrated together with the patterns for the preferred-oriented Ca-saturated samples.
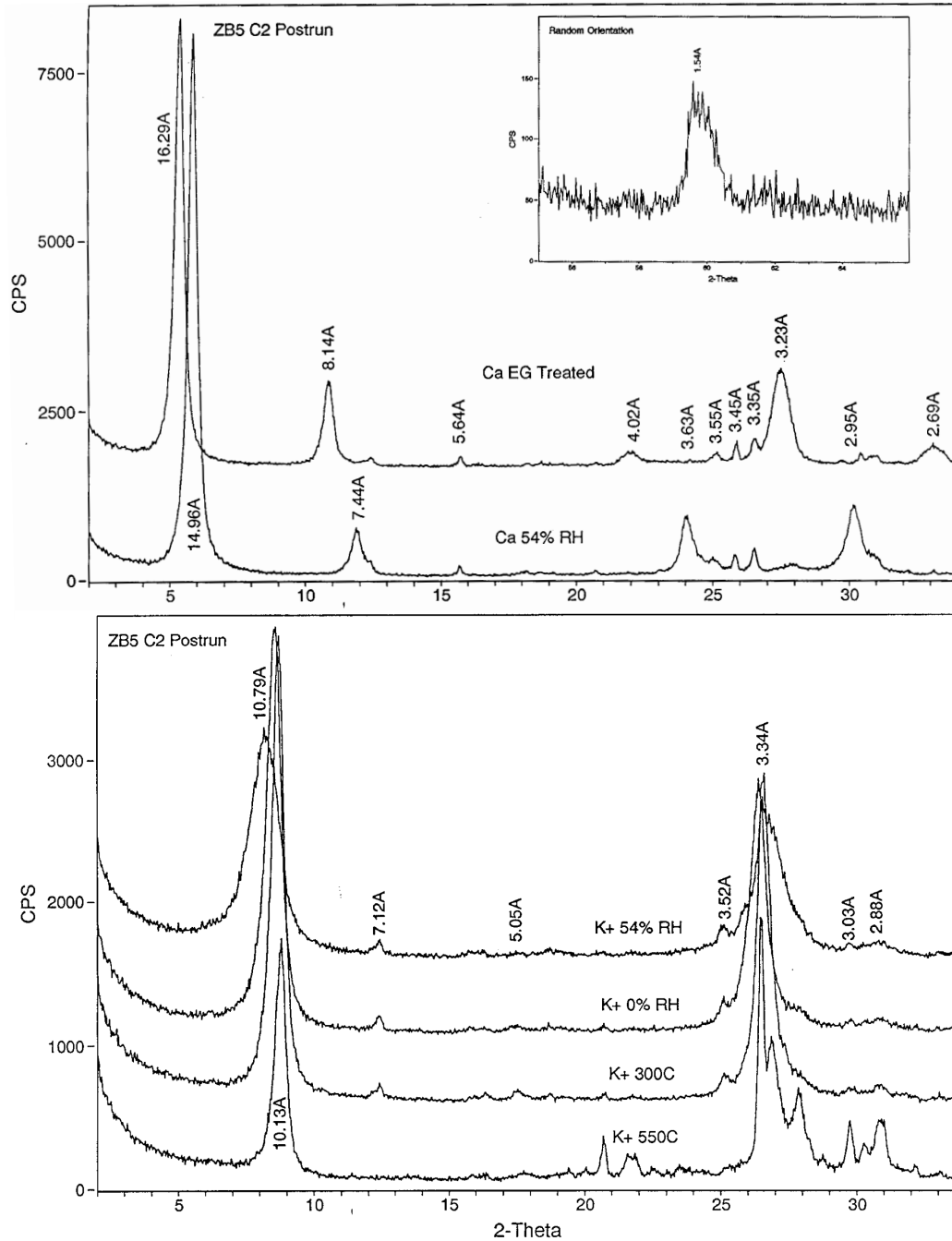
Fig. S3. XRD patterns of the <2 μm size-fraction of post-run solid ZB5C2 with different pre-treatment: Ca-saturation at 54% RH, vapour saturation with ethylene glycol (EG), and K-saturation at 0% RH and 54% RH, followed by heating to 300°C and then 550°C (from Zhou et al., 1994). The 06 band diffraction pattern for randomly oriented samples is also illustrated together with the patterns for the preferred-oriented Ca-saturated samples.
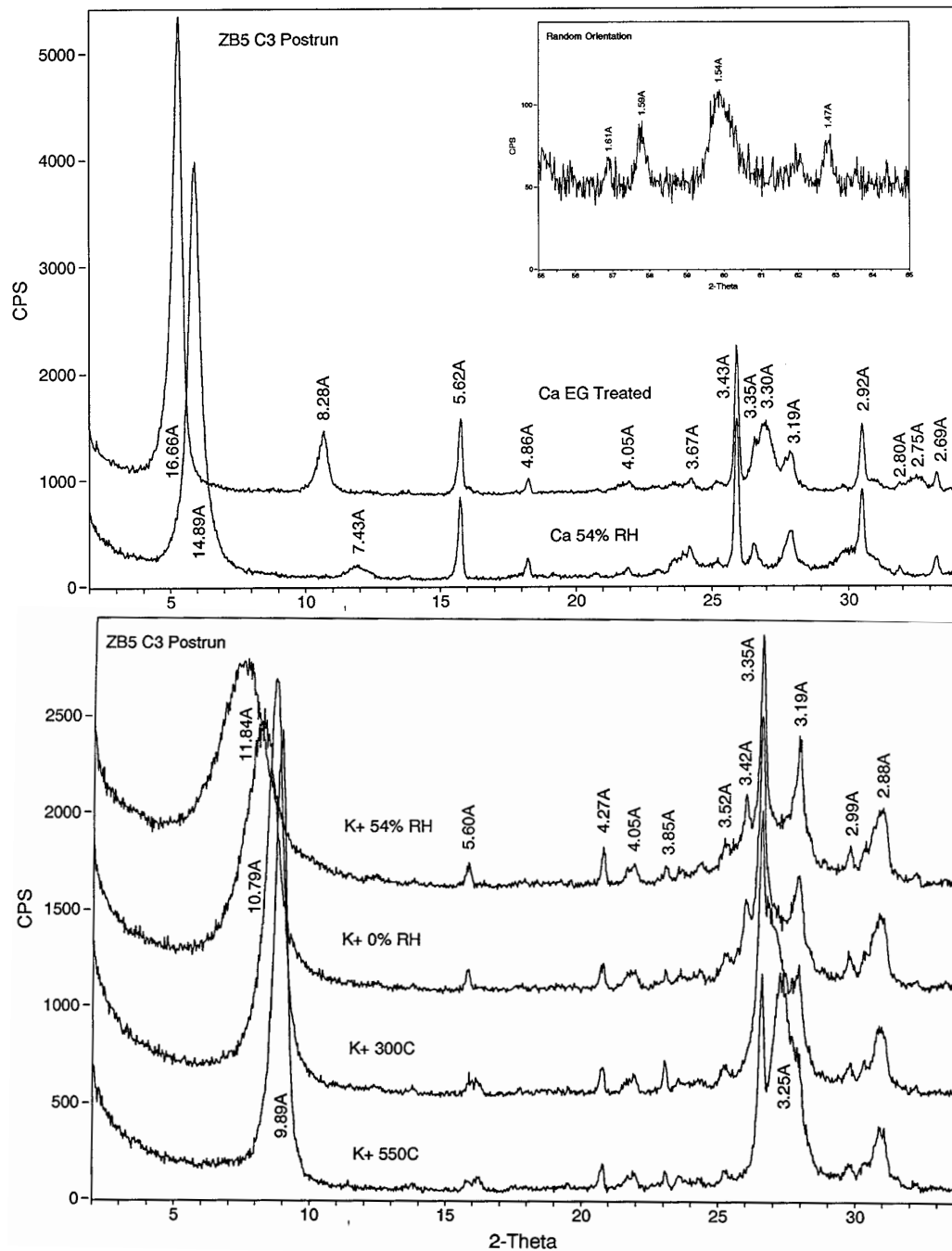
Fig. S4. XRD patterns of the <2 μm size-fraction of post-run solid ZB5C3 with different pre-treatment: Ca-saturation at 54% RH, vapour saturation with ethylene glycol (EG), and K-saturation at 0% RH and 54% RH, followed by heating to 300°C and then 550°C (from Zhou et al., 1994). The 06 band diffraction pattern for randomly oriented samples is also illustrated together with the patterns for the preferred-oriented Ca-saturated samples.
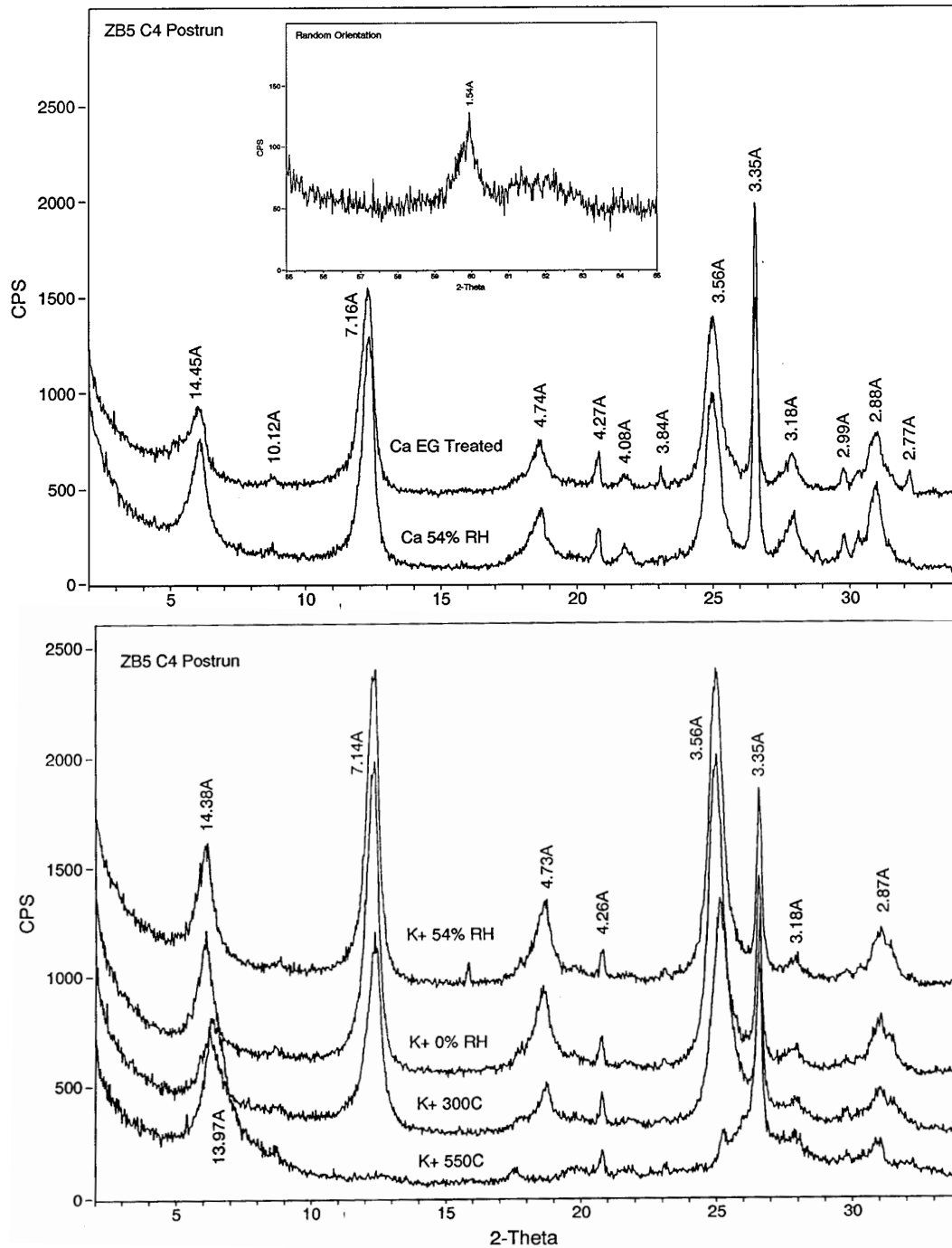
Fig. S5. XRD patterns of the <2 µm size-fraction of post-run solid ZB5C4 with different pre-treatment: Ca-saturation at 54% RH, vapour saturation with ethylene glycol (EG), and K-saturation at 0% RH and 54% RH, followed by heating to 300°C and then 550°C (from Zhou et al., 1994). The 06 band diffraction pattern for randomly oriented samples is also illustrated together with the patterns for the preferred-oriented Ca-saturated samples.

Fig. S6. XRD patterns of the <2 µm size-fraction of ZB6-prerun with different pre-treatment: Ca-saturation at 54% RH, vapour saturation with ethylene glycol (EG) (from Zhou et al., 1994). The 06 band diffraction pattern for randomly oriented samples is also illustrated together with the patterns for the preferred-oriented Ca-saturated samples.
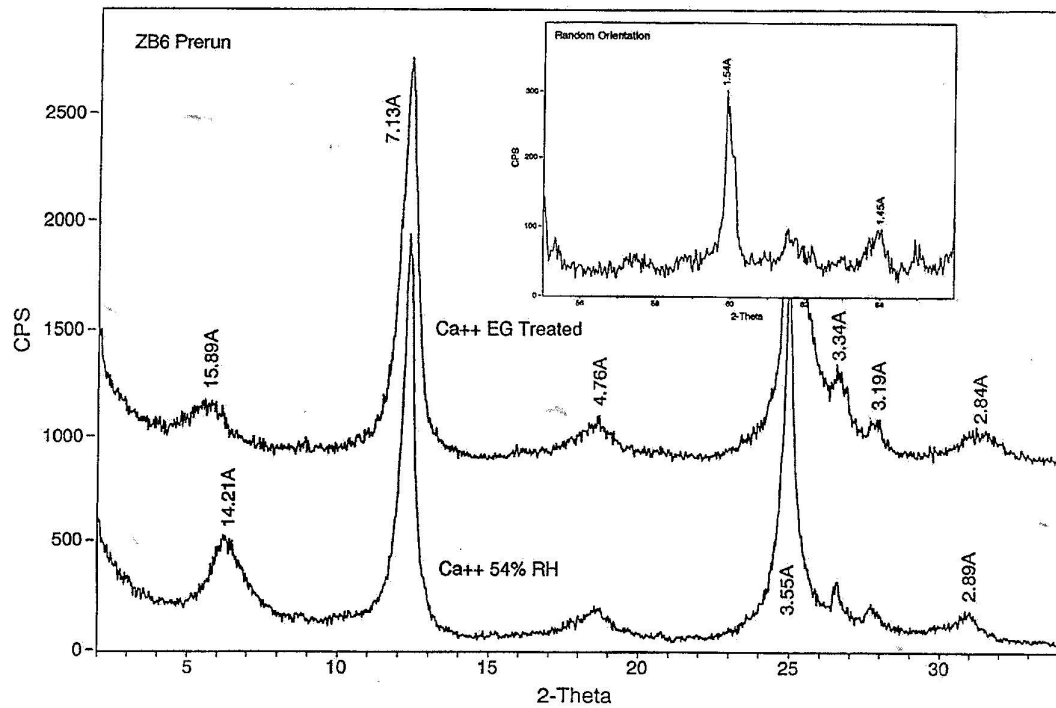
Fig. S7. XRD patterns of the <2 μm size-fraction of post-run solid ZB6C1 with different pre-treatment: Ca-saturation at 54% RH, vapour saturation with ethylene glycol (EG), and K-saturation at 0% RH and 54% RH, followed by heating to 300°C and then 550°C (from Zhou et al., 1994). The 06 band diffraction pattern for randomly oriented samples is also illustrated together with the patterns for the preferred-oriented Ca-saturated samples.
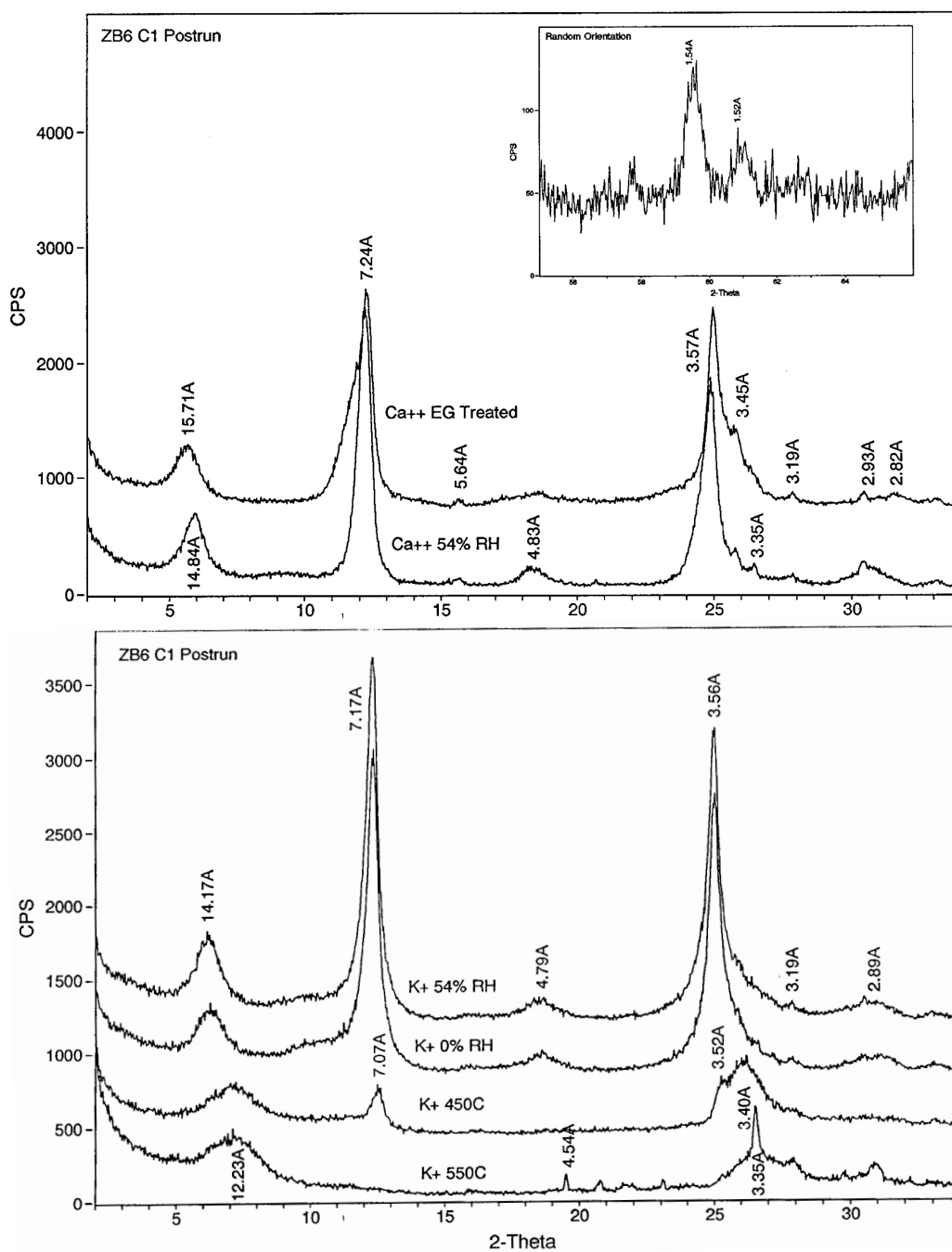
Fig. S8. XRD patterns of the <2 μm size-fraction of post-run solid ZB6C2 with different pre-treatment: Ca-saturation at 54% RH, vapour saturation with ethylene glycol (EG), and K-saturation at 0% RH and 54% RH, followed by heating to 300°C and then 550°C (from Zhou et al., 1994). The 06 band diffraction pattern for randomly oriented samples is also illustrated together with the patterns for the preferred-oriented Ca-saturated samples.
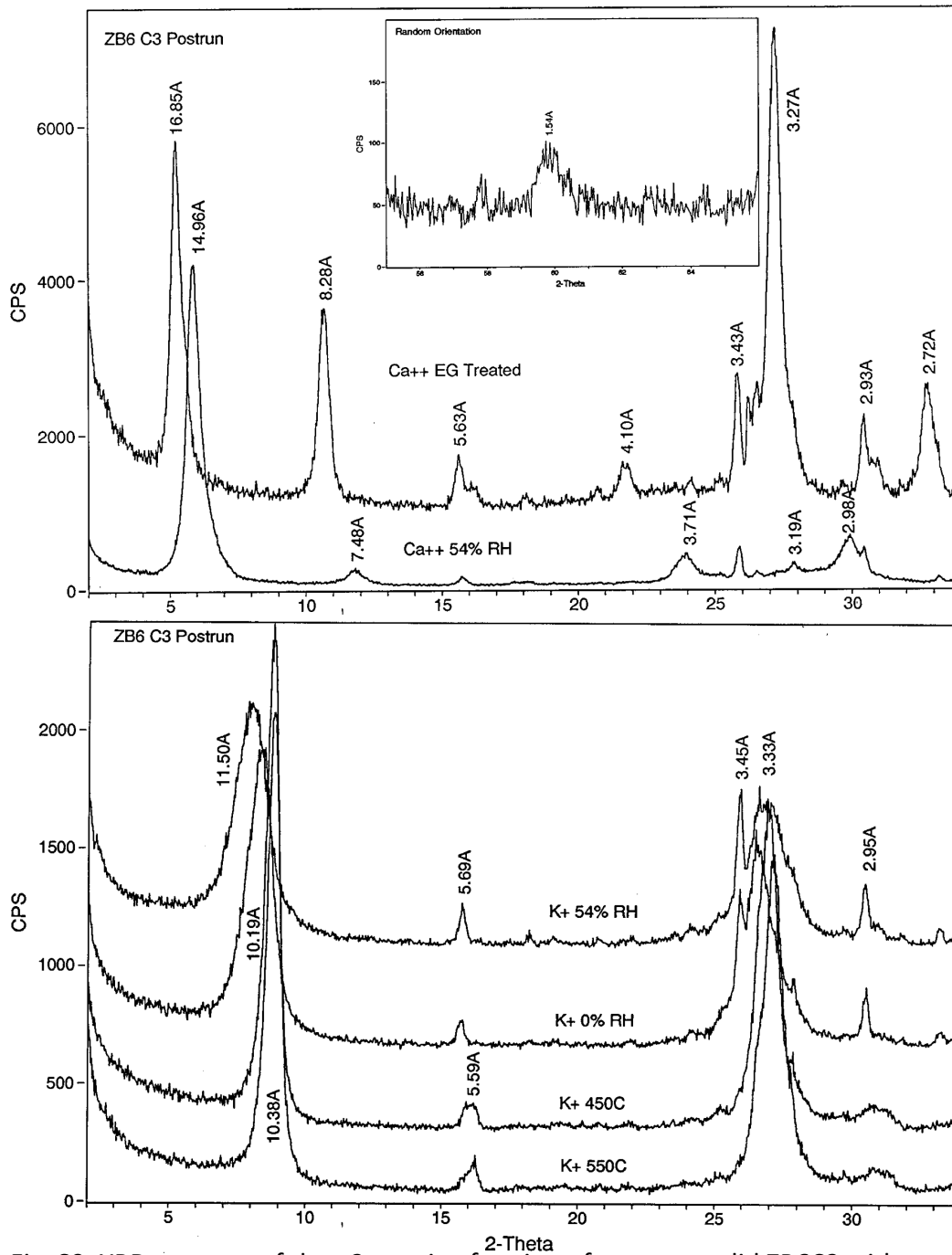
Fig. S9. XRD patterns of the <2 μm size-fraction of post-run solid ZB6C3 with different pre-treatment: Ca-saturation at 54% RH, vapour saturation with ethylene glycol (EG), and K-saturation at 0% RH and 54% RH, followed by heating to 300°C and then 550°C (from Zhou et al., 1994). The 06 band diffraction pattern for randomly oriented samples is also illustrated together with the patterns for the preferred-oriented Ca-saturated samples.
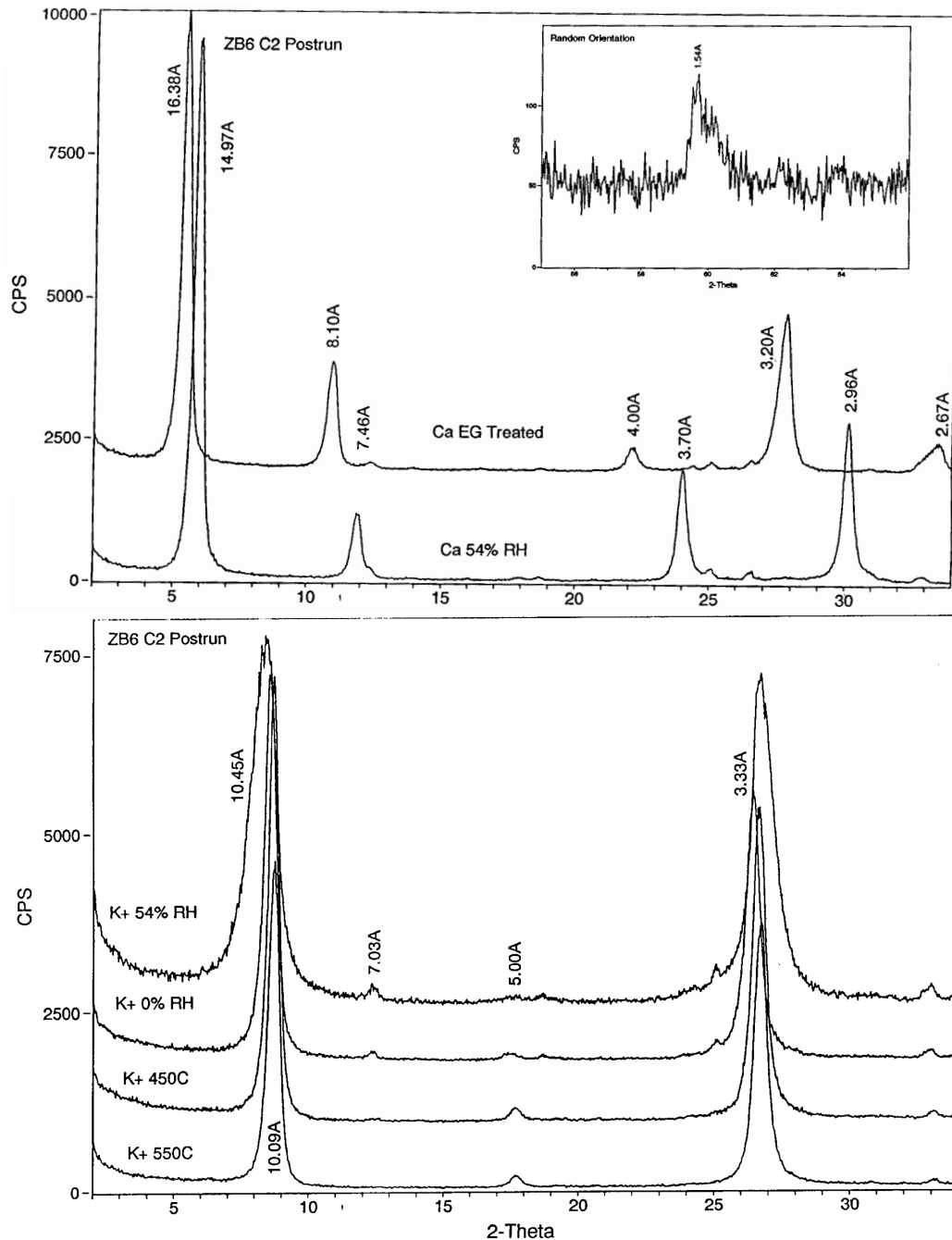
Fig. S10. XRD patterns of the <2 μm size-fraction of post-run solid ZB6C4 with different pre-treatment: Ca-saturation at 54% RH, vapour saturation with ethylene glycol (EG), and K-saturation at 0% RH and 54% RH, followed by heating to 300°C and then 550°C (from Zhou et al., 1994). The 06 band diffraction pattern for randomly oriented samples is also illustrated together with the patterns for the preferred-oriented Ca-saturated samples.
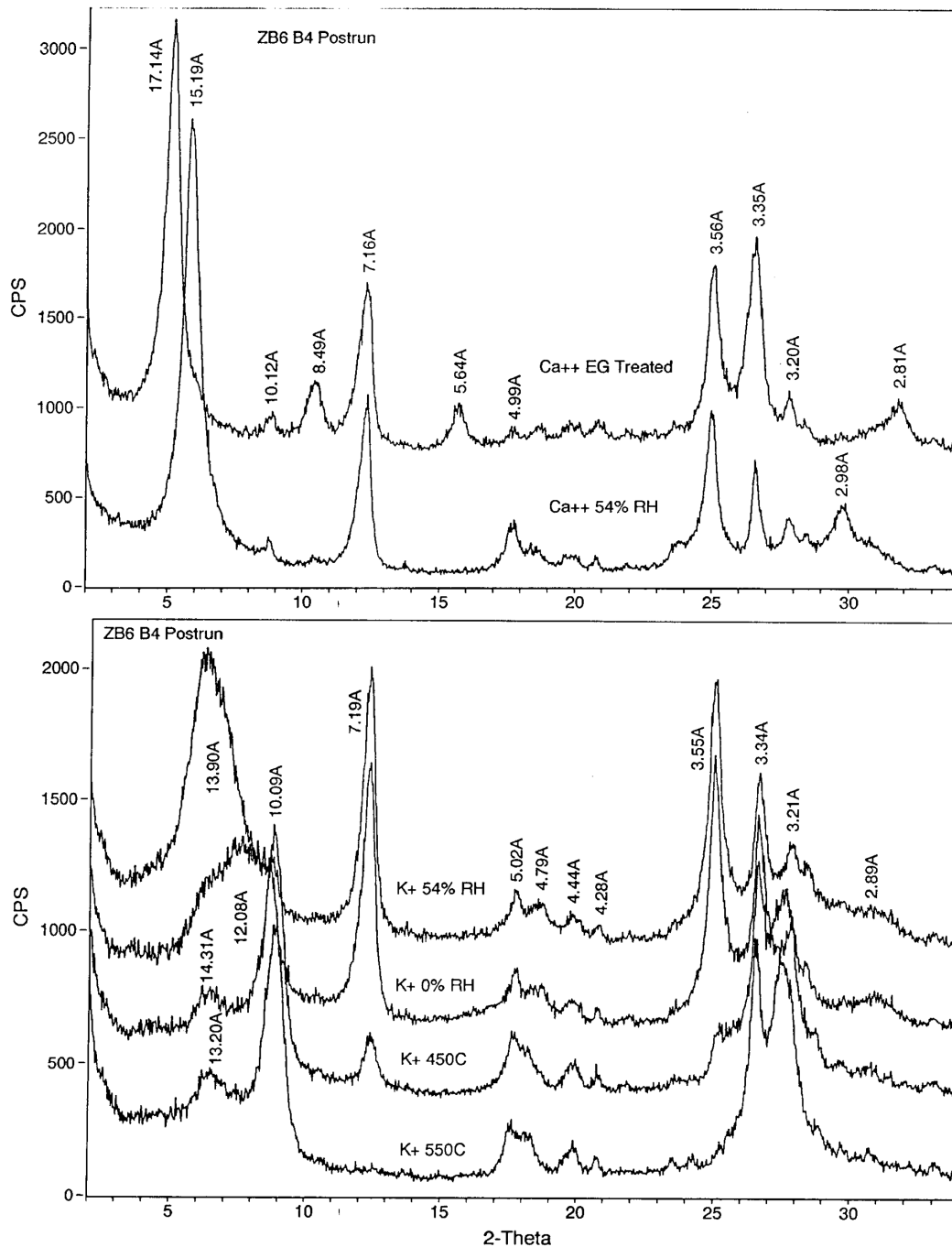
Supplementary Tables S1-S3. (Reproduced in modified form by permission of Alberta Innovates)

Table S1 Normalized AEM data for berthierine in sample ZB6 *

Sample ID	1	2	2	4	5	6	7	8	9	10
Si	1.564	1.619	1.612	1.659	1.723	1.691	1.548	1.568	1.510	1.615
Al^{IV}	0.437	0.381	0.389	0.342	0.277	0.309	0.453	0.432	0.490	0.385
Al^{VI}	0.667	0.649	0.746	0.613	0.691	0.706	0.656	0.676	0.649	0.680
Fe^{2+}	1.475	1.530	1.451	1.492	1.338	1.472	1.618	1.535	1.498	1.494
Mg	0.623	0.535	0.471	0.521	0.617	0.523	0.578	0.639	0.774	0.649
Mn	0.000	0.049	0.042	0.000	0.000	0.013	0.000	0.000	0.000	0.000
Cr	0.000	0.079	0.056	0.031	0.029	0.027	0.021	0.014	0.000	0.000
Ti	0.000	0.000	0.000	0.104	0.060	0.000	0.000	0.000	0.000	0.000
Ca	0.000	0.000	0.000	0.000	0.000	0.000	0.017	0.000	0.000	0.061
K	0.044	0.000	0.071	0.000	0.000	0.000	0.020	0.024	0.000	0.000
Na	0.197	0.000	0.000	0.000	0.000	0.107	0.000	0.000	0.000	0.000

* After Zhou et al. (1994), and calculated on the basis of $O_5(OH)_4$.

Table S2 Normalized AEM and EMP data for Fe-rich swelling clays *

Sample ID	EMP 1	EMP 2	EMP 3	EMP 4	AEM 1	AEM 2	AEM 3	AEM 4
Si	5.717	5.681	5.989	6.105	5.875	5.757	6.460	6.248
Al^{IV}	2.283	2.319	2.001	1.895	2.125	2.243	1.540	1.752
Al^{VI}	0.148	0.121	0.434	0.605	0.450	0.395	0.865	0.541
Fe	4.243	4.207	3.756	3.573	4.007	4.100	3.405	3.877
Mg	1.846	1.893	1.734	1.755	1.451	1.404	1.391	1.191
Cr	0.000	0.000	0.000	0.000	0.055	0.041	0.000	0.000
Mn	0.018	0.020	0.025	0.022	0.054	0.051	0.072	0.000
Ti	0.000	0.000	0.000	0.000	0.000	0.048	0.000	0.000
Ca	0.124	0.812	0.151	0.639	0.149	0.182	0.150	0.186
K	1.318	0.003	1.302	0.038	0.087	0.063	0.053	0.094
Na	0.060	0.089	0.073	0.063	1.270	1.206	0.855	1.525

AEM: analyzed by analytical electron microscope; all four analysis are done on ZB6C2.

EMP: analyzed by electron microprobe; EMP 1 was done on K-saturated ZB6C2,

      EMP 2 on Ca-saturated ZB6C2, EMP 3 on K-saturated ZB5C2 and EMP 4 on Ca-saturated ZB5C2;

      each of the reported EMP datasets are the average of three analyses.

* After Zhou et al. (1994), and calculated on the basis of $O_{20}(OH)_4$.

Table S3 Normalized AEM data of chlorite in sample ZB6C4 *

ID	1	2	3	4	5	6	7	8	9	10
Si	3.298	3.081	3.033	3.024	3.395	2.783	3.530	3.239	2.618	3.377
Al^{IV}	0.703	0.919	0.968	0.976	0.606	1.217	0.470	0.762	1.383	0.624
Al^{VI}	2.123	1.960	1.443	1.964	2.512	1.013	2.386	2.038	0.706	2.140
Fe	2.481	2.469	2.984	2.780	1.885	1.595	1.923	2.392	2.006	2.075
Mg	0.641	0.822	1.242	0.621	0.521	0.353	0.459	0.716	0.410	0.921
Cr	0.000	0.000	0.000	0.000	0.000	0.000	0.000	0.000	0.000	0.000
Mn	0.000	0.063	0.000	0.000	0.062	0.000	0.000	0.000	0.053	0.000
Ti	0.000	0.000	0.000	0.000	0.000	0.000	0.093	0.054	0.054	0.000
Ca	0.000	0.000	0.000	0.076	0.000	0.000	0.000	0.000	0.000	0.000
K	0.091	0.077	0.190	0.134	0.134	0.283	0.179	0.221	0.120	0.214
Na	0.000	0.256	0.000	0.000	0.000	0.000	0.000	0.000	0.000	0.000

* After Zhou et al., (1994), and calculated on the basis of $O_{10}(OH)_8$.